



**Calhoun: The NPS Institutional Archive**  
**DSpace Repository**

---

Theses and Dissertations

1. Thesis and Dissertation Collection, all items

---

2009-12

# Applications of marine radar wave observation systems

Meskill, Shay J.

Oregon Oregon State University

---

<http://hdl.handle.net/10945/4299>

*Downloaded from NPS Archive: Calhoun*



Calhoun is a project of the Dudley Knox Library at NPS, furthering the precepts and goals of open government and government transparency. All information contained herein has been approved for release by the NPS Public Affairs Officer.

**Dudley Knox Library / Naval Postgraduate School**  
**411 Dyer Road / 1 University Circle**  
**Monterey, California USA 93943**

<http://www.nps.edu/library>

# Applications of Marine Radar Wave Observation Systems

---

Masters of Science Project Report

Shay J. Meskill  
01/13/2010

Masters of Science technical report of Shay J Meskill presented on December 15<sup>th</sup>, 2009

Approved

---

Merrick C. Haller, Major Professor, representing Civil Engineering

---

Scott A. Ashford, Head of School of Civil and Construction Engineering

I understand that my technical report will become a part of the permanent collection of Oregon State University libraries. My signature authorizes the release of my project to any reader upon request.

---

Shay J. Meskill, author

# Table of Contents

---

|                                                  |    |
|--------------------------------------------------|----|
| 1. Abstract .....                                | 6  |
| 2. Introduction.....                             | 8  |
| 3. Background.....                               | 8  |
| 3.1 RADAR .....                                  | 8  |
| 3.2 Nearshore Radar Systems .....                | 10 |
| 3.3 X-Band Radar .....                           | 13 |
| 4. Shore-Based Station -- Newport.....           | 14 |
| 4.1 Site Conditions -- Newport.....              | 14 |
| 4.2 Set Up -- Newport.....                       | 16 |
| 4.3 Data Processing -- Newport Beach Study ..... | 17 |
| 4.4 Results -- Newport Beach Study.....          | 22 |
| 4.5 Analysis -- Newport Beach Study .....        | 25 |
| 4.7 Results -- Newport Jetty Study.....          | 32 |
| 4.8 Analysis -- Newport Jetty Study .....        | 35 |
| 5. Shipboard Observations -- Reedsport.....      | 40 |
| 5.1 Site Conditions -- Reedsport.....            | 40 |
| 5.2 Set Up -- Reedsport .....                    | 41 |
| 5.3 Data Processing -- Reedsport.....            | 42 |
| 5.4 Results -- Reedsport.....                    | 45 |
| 5.5 Analysis -- Reedsport .....                  | 48 |
| 6. Conclusion .....                              | 48 |
| 6.1 Shore-Based Station -- Newport.....          | 48 |
| 6.2 Shipboard Observations -- Reedsport.....     | 49 |
| 6.3 Additional Research.....                     | 49 |
| 7. References.....                               | 50 |
| 8.1 Guy Wire Design .....                        | 52 |
| 8.2 Matlab Script .....                          | 53 |

# List of Equations

---

|                                               |    |
|-----------------------------------------------|----|
| Equation 1: Radar Range .....                 | 8  |
| Equation 2: Radar Frequency .....             | 9  |
| Equation 3: Directional Power Density .....   | 14 |
| Equation 4: De-meaned Intensity .....         | 19 |
| Equation 5: Sine Window .....                 | 20 |
| Equation 6: Spectral Energy .....             | 20 |
| Equation 7: Average Spectral Energy.....      | 20 |
| Equation 8: Average Frequency .....           | 20 |
| Equation 9: Average Period.....               | 20 |
| Equation 10: Mean Intensity.....              | 31 |
| Equation 11: Mean Percent Intensity.....      | 31 |
| Equation 12: Standard Deviation.....          | 32 |
| Equation 13: Average Standard Deviation ..... | 32 |

# List of Figures

---

|                                                                               |    |
|-------------------------------------------------------------------------------|----|
| Figure 1: Oregon Coast.....                                                   | 6  |
| Figure 2: Radar Operation Steps.....                                          | 9  |
| Figure 3: HF Radar Return .....                                               | 12 |
| Figure 4: Buoy and Station Location.....                                      | 14 |
| Figure 5: Newport Radar Tower.....                                            | 15 |
| Figure 6: Newport Study Areas .....                                           | 15 |
| Figure 7: Newport Radar .....                                                 | 16 |
| Figure 8: Newport Radar Control and Acquisition.....                          | 16 |
| Figure 9: Radar Data Return Properties.....                                   | 16 |
| Figure 10: Nye Beach Study Area.....                                          | 18 |
| Figure 11: South Beach Study Area .....                                       | 19 |
| Figure 12: Newport Beach Processing Flow Chart .....                          | 20 |
| Figure 13: Newport Beach Results Flow Chart.....                              | 22 |
| Figure 14: Example Nye Beach Intensity Time Series.....                       | 23 |
| Figure 15: Example Nye Beach Energy Spectrum.....                             | 23 |
| Figure 16 September Nye Beach Average Period .....                            | 24 |
| Figure 17 September South Beach Average Period .....                          | 24 |
| Figure 18 September Nye and South Beach Double Running Average Period .....   | 25 |
| Figure 19 Nye and South Beach Average Period at Low Wave Angles .....         | 26 |
| Figure 20 Nye and South Beach Average Period at High Wave Angles.....         | 26 |
| Figure 21 Nye and South Beach Average Period at High Winds Speeds .....       | 27 |
| Figure 22 Nye and South Beach Average Period at Low Winds Speeds .....        | 27 |
| Figure 23 Radar Image at High Wind Speeds .....                               | 28 |
| Figure 24 Radar Image at Low Wind Speeds.....                                 | 28 |
| Figure 25 Wave Energy Spectrum at Low Wind Speeds (Original Study Area).....  | 29 |
| Figure 26 Wave Energy Spectrum at Low Wind Speeds (Alternate Study Area)..... | 29 |
| Figure 27 Nye Beach Wave Energy Spectrum at High Wind Speeds.....             | 30 |
| Figure 28 South Beach Wave Energy Spectrum at High Wind Speeds .....          | 30 |

|                                                                    |    |
|--------------------------------------------------------------------|----|
| Figure 29 Jetty Study Area .....                                   | 31 |
| Figure 30 Jetty Data Processing Flow Chart .....                   | 32 |
| Figure 31 Jetty Radar Image.....                                   | 33 |
| Figure 32 Jetty Mean Intensity Image .....                         | 33 |
| Figure 33 Jetty Heavy Wave Breaking.....                           | 34 |
| Figure 34 Jetty Minimal Wave Breaking .....                        | 34 |
| Figure 35 Jetty Mean Intensity and Average Standard Deviation..... | 35 |
| Figure 36 Jetty Average Standard Deviation vs Tide (MLLW).....     | 35 |
| Figure 37 Jetty Average Standard Deviation vs Wave Height.....     | 36 |
| Figure 38 Jetty Average Standard Deviation vs Wind Speed.....      | 36 |
| Figure 39 Jetty Average Mean Intensity vs Wave Height.....         | 37 |
| Figure 40 Jetty Image at Low Wave Heights .....                    | 37 |
| Figure 41 Jetty Mean Intensity at Low Wave Heights .....           | 38 |
| Figure 42 Jetty Image at High Wave Heights.....                    | 38 |
| Figure 43 Jetty Mean Intensity at High Wave Heights.....           | 39 |
| Figure 44 Reedsport Wave Energy Array Site .....                   | 39 |
| Figure 45 Umpqua Offshore Buoy 46229 Location.....                 | 41 |
| Figure 46 Miss Linda Radar .....                                   | 40 |
| Figure 47 Charter Boat Miss Linda.....                             | 40 |
| Figure 48 VGA2USB .....                                            | 41 |
| Figure 49 Miss Linda Data Recording.....                           | 42 |
| Figure 50 Reedsport Results and Location.....                      | 42 |
| Figure 51 September Study Area.....                                | 43 |
| Figure 52 October Study Area.....                                  | 43 |
| Figure 53 Reedsport Data Processing Flow Chart.....                | 44 |
| Figure 54 September Reedsport Wave Energy Spectrum - 1 .....       | 45 |
| Figure 55 September Reedsport Wave Energy Spectrum - 2 .....       | 45 |
| Figure 56 September Reedsport Wave Energy Spectrum - 3 .....       | 46 |
| Figure 57 October Reedsport Wave Energy Spectrum - 1 .....         | 46 |
| Figure 58 October Reedsport Wave Energy Spectrum - 2 .....         | 47 |
| Figure 59 October Reedsport Wave Energy Spectrum - 3 .....         | 47 |

## List of Tables

|                                                        |    |
|--------------------------------------------------------|----|
| Table 1 Radar Classification (Remer 1997) .....        | 10 |
| Table 2 Reedsport Results Compared to Buoy 46229 ..... | 48 |

## **1. Abstract**

This project utilized both shore-based and shipboard commercial marine radar technology to collect wave statistics. In the first application a shore-based system was installed at Yaquina Bay in Newport, Oregon in order to collect real-time wave information. This information was collected under the auspices of the Northwest Association of Networked Ocean Observing Systems (NANOOS) and will be used in ongoing studies on wave-current interaction. In the second application, a shipboard radar system was utilized to develop processing procedures and algorithms for collecting offshore wave data. These shipboard collections were in support of the environmental baseline study of the Reedsport Wave Energy Site, funded by the Oregon Wave Energy Trust (OWET).

## 2. Introduction

The foundation of every engineering solution is to first quantify the existing site conditions. As the requirements for coastal structures grow, the methods for acquiring the coastal site conditions must evolve as well. Compared to inland-based projects, the coastal region presents some additional challenges such as ever changing wave and tidal conditions. The traditional in-situ methods for observing these conditions may be more difficult to execute due to lack of access to the site. The use of marine radar (Radio Detection And Ranging) remote observation systems can significantly reduce site access limitations, while providing real-time observations over a large study area in support a variety of applications.

In this project, the two applications of remote radar observations utilized both shore-based and shipboard collections. Figure 1 displays the Oregon coast and marks the locations of the two studies. In the shore-based study a radar station was established on the south jetty in Newport, OR. The information collected from this site collected hourly wave images that will be provided to the Northwest Association of Networked Ocean Observing Systems (NANOOS) website. NANOOS acts as a collection point for ocean observations for the United States Northwest Pacific area, providing coastal environmental data to scientists and other interested parties. This data was also used as a proofing study to show that wave spectrum can be developed using radar images. The data will also be used to capture tidal effects on the wave spectra that will later be used to validate wave-modeling software.

In the shipboard application the radar data was taken directly from the operating radar of the U.S. charter boat Miss Linda. The images were captured while underway using a VGA to USB conversion device and software. The shipboard data will be used to establish baseline wave conditions at the Reedsport Wave Energy Site.



Figure 1: Oregon Coast



### 3. Background

Remote sensing of coastal processes has made significant development over the past few decades as the technological advances in monitoring devices has allowed for more opportunities in the field. The use of photography and videography can be applied to estimate coastal changes. The ARGUS Beach Monitoring Stations (ABMS) is a principle photography system developed at the Oregon State University Coastal Imaging Laboratory (CIL). The U.S. Geological Survey and U.S. Army Corps of Engineers use ABMS to monitor longer-term processes such as wave run up and beach erosion. The use of Light Detection and Ranging (LIDAR) technology has been applied to many fields, including mapping coastal bathymetry with accuracy on the scale of millimeters. The LIDAR system is very impressive in recording static spatial data but is not typically used to capture moving fluids, i.e. waves. When monitoring short-term phenomena such as waves the most promising method is the use of radar.

#### 3.1 RADAR

Based off a discovery by Heinrich Hertz, German engineer Christian Hulsmeyer developed a radar early warning system for ships in 1904. However, the use of radar did not become popular until 1935 when Robert Watson-Watt discovered radar's usefulness in tracking airplanes while trying to develop a "death ray" for the British Air Ministry. The technology blossomed during World War II in military applications and later became the standard for commercial transportation. The principles of radar are based off simple speed calculations. The radar system will transmit a pulse of energy in a known direction from a known origin. The pulse will travel thru the atmosphere at a known speed, reflect off an object and a portion of the energy will return to the radar antenna. Based off the time that the energy pulse returns the radar can pinpoint the range of the object being one half the time over speed shown in Equation 1.

$$R=T/(2C) \quad \text{(Equation 1)}$$

R= Range

T= Time

C= Speed, speed of light

The steps utilized in the operation of modern radar systems are shown in Figure 2. The process begins at the digital waveform generator in which the desired waveform is created based on expected characteristics of the targets, the demands of Moving Target Indication (MTI) and Electromagnetic Compatibility (EMC). The waveform generator sends an Intermediate

Frequency (IF) signal to the mixer component that creates the Radio Frequency (RF) in a process called upconversion. The RF signal is then boosted by the power amplifier and then transmitted thru the duplexer and antenna. The duplexer utilizes the antenna to both transmit and receive signals. When in receiving mode the duplexer sends the received signal thru a Low Noise Amplifier (LNA) that boosts the desired signal. The mixer then changes the received RF signal to IF via downconversion and the signal is then processed. The processing system utilizes very complex digital processing filters to convert the raw signals into a simplified array for viewing.

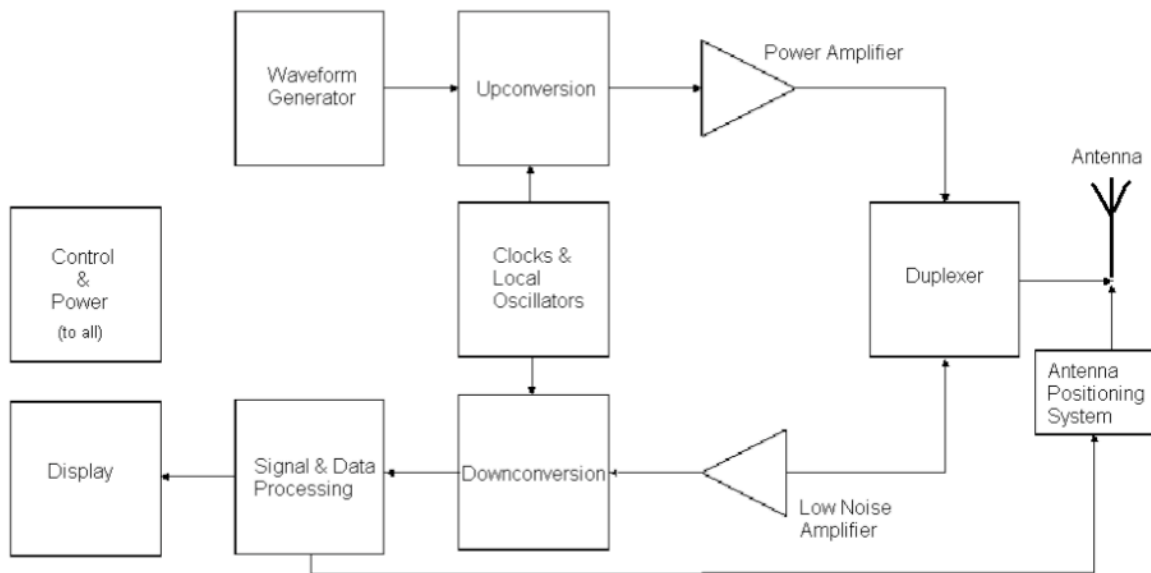


**Figure 2: Radar Operation Steps**

The type of radar system is characterized by its bandwidth based on the pulse frequency and corresponding wavelength. The frequency is related to wavelength by multiplying its inverse by the speed of the signal shown in Equation 2. In this case the signal is traveling at the speed of light. Table 1 shows the distribution of radar classifications.

$$f = C/\lambda \quad \text{(Equation 2)}$$

$f$  = Frequency  
 $C$  = Speed, speed of light  
 $\lambda$  = Wavelength

**Table 1 Radar Classification (Remer 1997)**

| <b>Band</b> | <b>Frequency</b> | <b>Wavelength</b> |
|-------------|------------------|-------------------|
| HF          | 3-30 MHz         | 10-100 m          |
| VHF         | 30-300 MHz       | 1-10 m            |
| UHF         | 300 MHz-1 GHz    | 30 cm-1 m         |
| L-band      | 1-2 GHz          | 15-30 cm          |
| S-band      | 2-4 GHz          | 7.5-15 cm         |
| C-band      | 4-8 GHz          | 3.75-7.5 cm       |
| X-band      | 8-12 GHz         | 2.5-3.75 cm       |
| Ku-band     | 12-18 GHz        | 1.67-2.5 cm       |
| K-band      | 18-27 GHz        | 1.11-1.67 cm      |
| Ka-band     | 27-40 GHz        | 7.5 mm-1.11 cm    |
| V-band      | 40-75 GHz        | 4-7.5 cm          |
| W-band      | 75-110 GHz       | 2.7-4 mm          |
| mm-band     | 110-300 GHz      | 1-2.7 mm          |

Another notable characteristics of a given radar system is resolution. Radar resolution can be broken down into two components azimuthal and range. Azimuthal resolution defines the radars capability to discern between two objects side-by-side. The azimuthal resolution can only be as accurate as one pulse beam width, which is a function of distance. Because the beam is transmitted at its minimal beam width targets are seen with more accuracy at close distances than at further distances. As the pulse beam travels farther the returning signal will become more distorted. Range resolution describes the radar's ability to separate objects along the beams path. Targets must be separated by at least half the pulse length in order to be seen separately. However, the pulse length does not change with distance so that the range resolution is constant with distance.

### **3.2 Nearshore Radar Systems**

The characteristics of a given radar limits its applications. Within the field of nearshore observations there are several major types of radar technology used: Space-borne (satellite) radar, High Frequency (HF) radar, and X-Band radar. The Space-borne systems can be broken down further into three main groups consisting of Synthetic Aperture Radar (SAR), Radar

Altimeter (RA), and Scatterometer. The SAR version utilizes satellites (space-borne) or aircraft (air-borne) platforms to emit multiple radar signals at the same general location relative to the observed area. For example, within the time it takes for a radar impulse to travel back and forth, a slow flying aircraft does not change significantly in position compared to the overall coastline that it is mapping. Taking this into consideration a series of radar returns can be combined to create a continuous series of data points from one origin. This creates a ‘synthetic aperture’ effect as if the original signal were gathered simultaneously from an extremely large antenna. Spatial data gathered using these techniques can be as accurate as 10 centimeters. Due to its high accrual and operational expenses the majority of SAR technology is utilized by government agencies in geological mapping, maritime movement monitoring and numerous other applications including military purposes.

The RA radar system is similar to that of the SAR system yet less advanced and therefore less accurate. A typical RA application is providing the Ground Proximity Warning System (GPWS) in commercial aircraft during flight. More advanced space-borne RA systems monitor large ocean activities such as tides and currents. Scatterometer systems filter out the strong signals from multiple readings to isolate the “noise”. The noise readings can then be translated into wind interference that becomes the primary purpose of the Scatterometer, which is to monitor ocean winds.

HF radar systems are being used for many coastal observations such as tracking oil spills, coastal discharges and marine populations. HF radar systems operate in the lowest of frequency bands. This leads to higher wavelengths and therefore less resolution in the radar data. However, the HF systems provide a longer range and are capable of making observations around obstacles or beyond line-of-sight (BLOS). These characteristics make the HF system a primary affordable option for observing coastal phenomena over a great distance from shore.

A large part of the scientific HF radar applications are in the field of surface current measurement. By transmitting a pulse from one HF antenna and receiving from another, the HF system can be used to determine the change in frequency. This ‘doppler shift’ will then provide enough information to determine the speed of the water (Terrill, 2009). Using a network of HF

stations it is possible to accurately map the ocean currents up to 150km from the coastline. Near real-time databases are available thru communities of scientists such as the Integrated Ocean Observing System (IOOS), NANOOS and California Coastal Ocean Current Monitoring Program (COCMP).

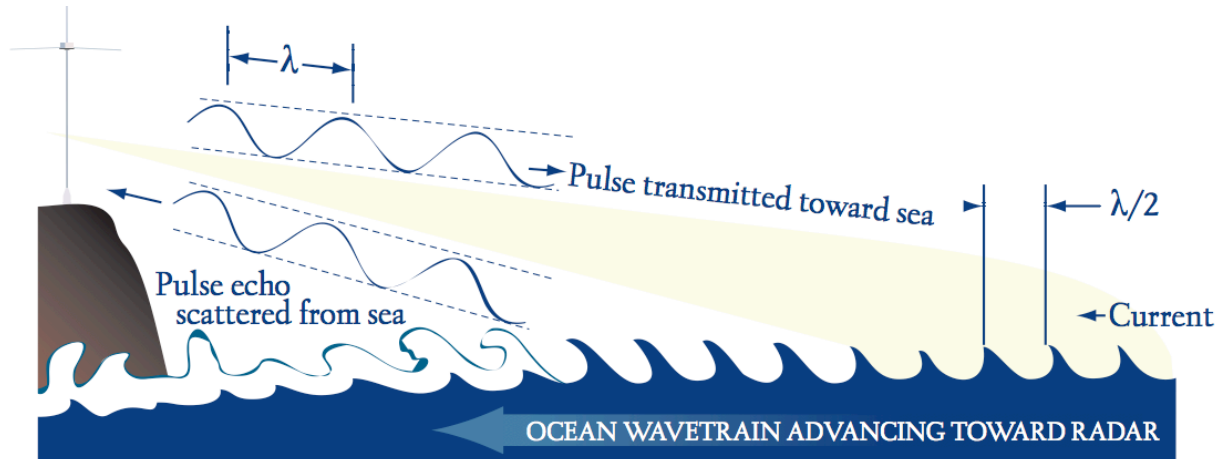


**Figure 3: HF Radar Return**

The purpose of this study is to describe wave spectra and therefore requires an accurate means of measuring individual waves. For this level of detail a smaller radar wavelength is required and X-band has been the most commonly used over the last few decades. X-band radar remote sensing began in the late 20<sup>th</sup> century by combining radar data with aerial pictures to hand calculating wave information. As technology advanced, images were digitally scanned and processed. By the turn of the century the data was loaded directly from the radar as seen in the development of the Wave and Surfaces Current Monitoring System (WAMOS).

Specifically relating to this study J D Lentine (2006) performed a X-band radar trial for Oregon State University titled *Nearshore Applications of Marine Radar*. Lentine utilized an onshore radar system at the Mouth of the Columbia River in Oregon and the U. S. Army Corps of Engineers (USACE) Field Research Facility (FRF) in Duck, North Carolina. In his study he found that “estimated radar periods and direction compared to in situ periods and direction showed good agreement for both field deployments”. He also noted that the wave conditions in the Pacific Northwest are ideal for remote sensing due to larger wave heights and longer periods.

### 3.3 X-Band Radar

X-Band Radar can observe individual wave trains through a phenomenon known as ‘backscatter’. Backscatter occurs when the transmitted radar pulse is reflected by the rough sea surface. If you were to look at a radar image of an open sea the only visible responses would be a tiny scattering of points. These points are known as ‘sea scatter’. What is known is that the backscatter is attributed to two interactions; specular and resonant reflections. Specular reflections are a result of the radar pulse bouncing off the surface of the water. The return intensity of specular reflection depends on the angle at which the pulse hits normally to the water surface, known as incidence angle. If the pulse hits the water surface perpendicularly, an incidence angle of zero, the specular reflection is at a maximum (Traenkman, 2008).

The second mode of reflection, resonant reflection, is a result of the interaction between the radar wavelength and the wavelength of the wave scatter. The water wavelengths of interest are the small capillary waves that occur at the water surface from wind action. Therefore the presence of wind is required for the observation of resonant reflections. For the purposes of nearshore observations the requirement for wind is often met.

Not only is it important to know how the radar is being reflected it is necessary to know how to interpret these reflections. Wave motions observed via X-Band radar are seen as intensity modulations caused by three sources; tilt angle, hydrodynamic and shadowing modulation. Tilt angle modulation is a result of specular reflection from the geometrical position of the wave. As the wave face rises towards the radar, the reflected intensity is increased. If the wave is traveling perpendicular to the radar beam the tilt angle modulation cannot be seen. Hydrodynamic modulation is caused by the changes in resonant reflections through the gravity wave motion. On the face of the gravity wave the capillary waves have an increased amplitude and smaller wavelength. Therefore more resonant reflections are observed on the face of the wave, similar to tilt angle modulation. Shadowing is a result of geometric obstructions preventing the reflections of objects immediately behind it. In the case of waves, it is typical to see the crest of the wave where the trough is not observed because it lies in the shadow zone of the crest.

In order to get the best wave observations the radar settings must be adjusted. Adjusting the antenna gain focuses the power density of the emitted radar beam. Equation 3 shows the basic equation of focused power density (Wolf).

$$S_g = S_u * G \quad \text{(Equation 3)}$$

$S_g$  = Directional Power Density  
 $S_u$  = Non Directional Power Density  
 $G$  = Antenna Gain

For the purposes of observing waves the gain must be increased so that the power density becomes directional and the ‘sea scatter’ is more apparent. The rate of sweep, speed at which the antenna rotates, must be maximized so that the wave observations are as continuous as possible. By monitoring the water surface continually the radar returns can be processed digitally to provide information about the wave height, wave length, wave period, wave direction and surface current.

#### **4. Shore-Based Station -- Newport**

In the Newport study an X-band radar system was established at a shore-based station in order to make nearshore observations. The purpose of these observations is to provide a proof of concept demonstration by calculating wave spectra information and comparing them to observed wave buoy data. This study will also provide a practical tool for local fisherman and scientists alike by publishing hourly radar wave images via the Northwest Association of Networked Ocean Observing Systems (NANOOS) website. Wave action in the jetty mouth will be related to tidal effects that will later be used to validate wave-modeling software.

##### **4.1 Site Conditions -- Newport**

The city of Newport surrounds the Yaquina Bay on the central coast of Oregon. Since the oyster beds were discovered in 1862 the city has been built around the fishing industry, which continues today (Discover Newport, 2009). Newport can be divided into three distinct areas consisting of the bay front, Nye Beach and the Highway 101 corridor. In order to protect the shipping channel into Yaquina Bay two rubble mound jetties were constructed in 1895 at the bay front. Today the north jetty sits at a length of 7,000 feet and the south jetty at 7,600 feet (Ward, 1988).

Wave information for the region is provided by National Oceanic and Atmospheric Administration (NOAA) thru a buoy at Stonewall Banks, Buoy 46050 (44°38'28" N 124°29'59" W). The Stonewall banks buoy is 20 nautical miles west of Yaquina Bay where the water depth is 123 meters, shown in Figure 4. Tidal and local atmospheric data is available from NOAA at Station 9435380 (44° 37.5' N 124° 2.5' W).

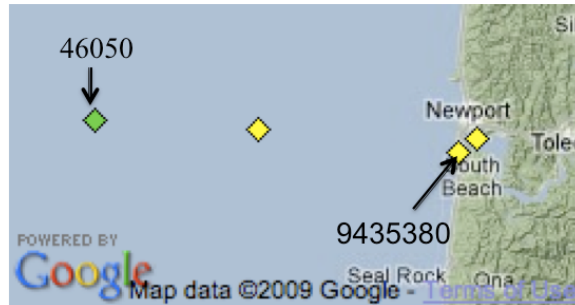


**Figure 4: Buoy and Station Location**

The shore-based radar was installed in the spring of 2009 at an existing OSU “blockhouse” at coordinates 44° 36' 48.7794” N and 124° 4' 3.864" W on the south jetty in Newport, OR. The facility is weather-protected with power supply and a 25-foot aluminum lattice tower shown in Figure 5. This facility also has a local area network connection to a server located at the Hatfield Marine Science Center 1 mile to the east. From this location the onshore radar covered all three distinct areas of Newport that will be referenced as follows; Nye Beach, jetty mouth (bay front), and South Beach (near the Highway 101 corridor) as shown in Figure 6.

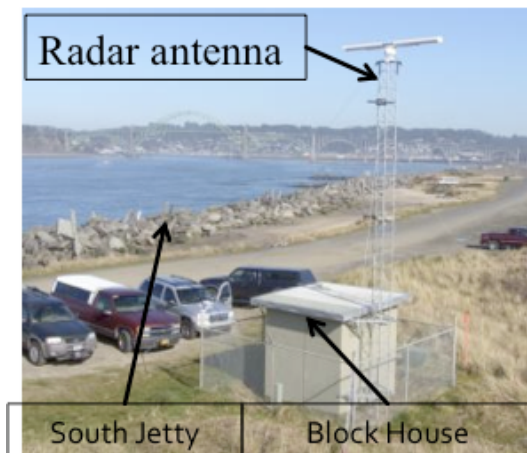


**Figure 5: Newport Radar Tower**

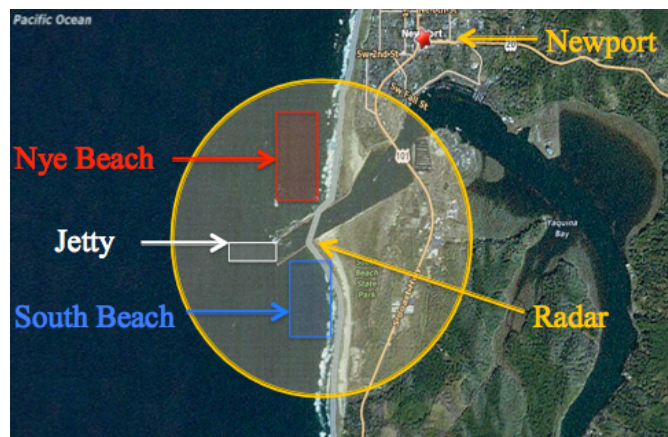


**Figure 6: Newport Study Areas**



## 4.2 Set Up -- Newport

The remote sensing system utilized for the shore-based Newport study consisted of: one X-Band marine radar, one radar control laptop computer, two data processing computers, and one network hub. Specifically a Si-Tex X-band marine radar version pc-25.9 was installed on top of the 25-foot aluminum tower as shown in Figure 7. Adding the radar antenna to the top of the tower added wind drag forces on the structure. In order to prevent structural damage a guy wire support system was installed. The required tensile loading of the guy wire system was 1,400lbs based off a 10 year wind speed of 150mph observed at the Newport Coast Guard Station. Six guy wires made of 1,800 lb rated aircraft restraint wire anchored by 2,500 lb rated ground screws at a 30-degree angle from the ground. Three guy wires were connected to a mounting plate at the top of the tower. Three wires connected to a point 2/3 the height of the tower as recommend by the US Marine Corps Field Antenna Handbook. The design details are shown in Appendix 8.1.



**Figure 7: Newport Radar**

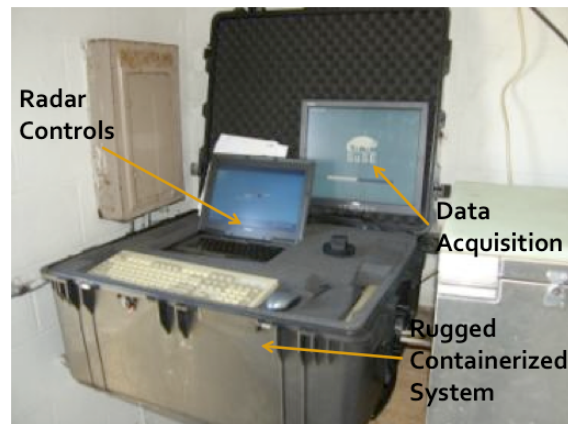


**Figure 8: Newport Radar Control and Acquisition**

A weatherproof transport case was customized in order to house the radar control laptop computer and the onsite processing computer as well as supporting components (control switch, radar power amplifier, etc...). Figure 8 shows the transport case and onsite operating components. The radar control laptop operated the radar using PSea Windplot II software. The onsite processing computer recorded the raw radar data every hour at 15 minutes past the hour for a duration of 15 seconds thru Crontab scripts. The complete record of data covered approximately four months, June to September 2009. Raw data was broadcast to an offsite processing computer using the network system provided by the Hatfield Marine Science Center.

Due to the minimal bandwidth of the wireless network system, the data had to be limited to 15 seconds of observations. The raw data was then processed using Matlab scripts and archived.

### 4.3 Data Processing -- Newport Beach Study

The raw data is stored in a binary format. Existing algorithms for Matlab were used to process the raw data. After the initial processing the portion of data used in this study consisted of the radar position, an observed rate of radar rotation, a vector of angles and a corresponding matrix of distances and pixel intensities for every time step. The vector of angles is recorded as Cube.Azi and the matrix of distances and pixels is Cube.data. Cube.Azi is the same for every time step where Cube.data records the new intensities for each time step so that:

|            |                  |           |              |
|------------|------------------|-----------|--------------|
| time=1     | Cube.Azi [300X1] | Cube.data | [916X300]    |
| time=2     | Cube.Azi [300X1] | Cube.data | [916X300]    |
| time(1:15) | Cube.Azi [300X1] | Cube.data | [916X300X15] |

The vector of radar angles (Cube.Azi) is the angle clockwise in the horizontal plane from the zero point of the radar shown in Figure 9. The angle of radar return is taken at whole number intervals (i.e. angles of 1-360 degrees leaves a vector of [360X1]). The matrix of distances and pixel intensities (Cube.data) are combined with each value of angles to create a 3-dimensional return. This polar coordinate system contains  $\theta$  (angle from radar zero),  $r$  (distance from radar) and  $i(\theta,r)$ (intensity of return at point  $(\theta,r)$ ).

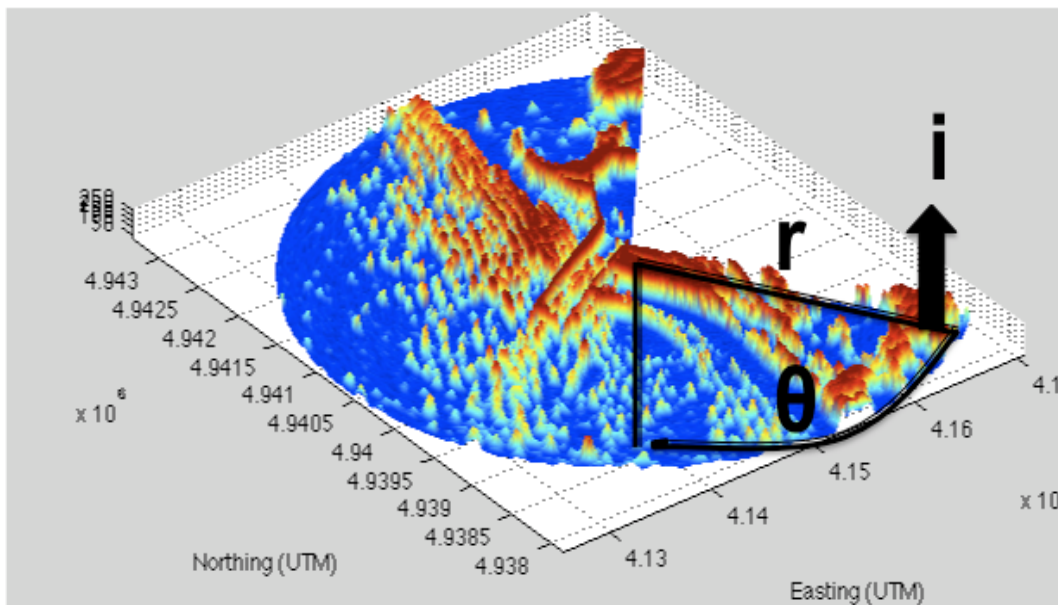


Figure 9: Radar Data Return Properties

The radar used in this study was not calibrated by in-situ wave heights. Therefore the resulting radar intensities do not carry any the units of any physical property. They simple represent the intensity of return, ranging from 0 to 256, over time. This concept will be discussed further in the Conclusions section. In order to calculate the frequencies observed as required in this study, the unit-less intensity readings will be appropriate.

The Newport data was processed in two different forms. First, study areas at Nye Beach and South Beach were used to compute average wave frequency and compare to observations at Buoy 46050. The average wave frequency must be used because the short duration time series only allow for a course spectral resolution in frequency space. The average period was calculated by first isolating the subset data for the given study area. The Nye Beach area was restricted to the intensities observed at  $\theta = [165:205]$  and  $r = [350:450]$ , South Beach was defined as  $\theta = [100:117]$  and  $r = [250:400]$ . Figures 10 and 11 show the Nye Beach and South Beach study areas compared to the complete radar return area.

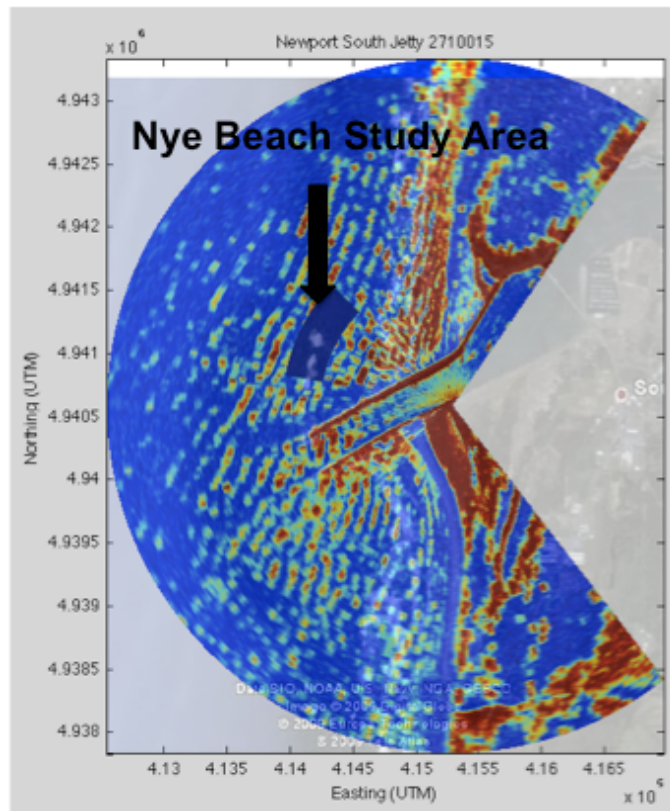
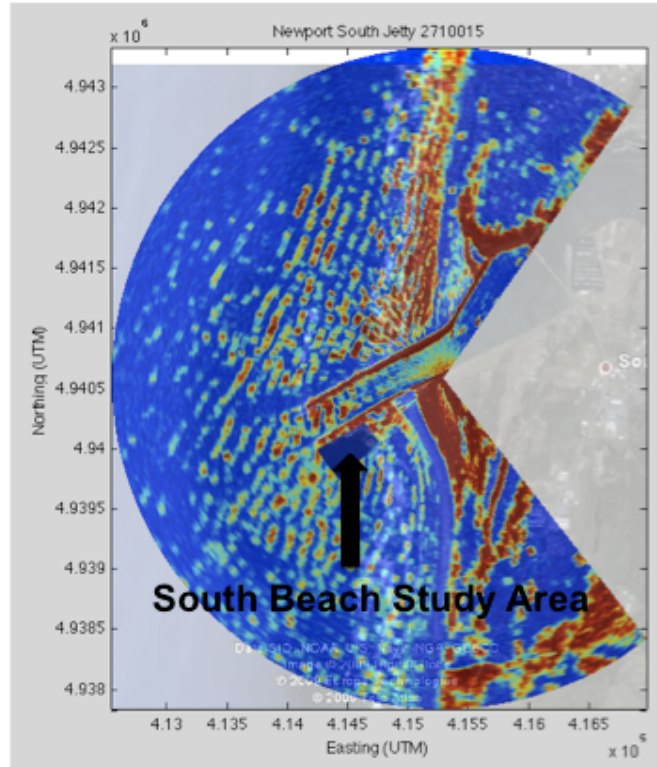


Figure 10: Nye Beach Study Area



**Figure 11: South Beach Study Area**

The process in which the data was processed is illustrated in Figure 12 and described below. In order to create a wave spectrum we use the 15 point time series each pixel location  $(\theta, r)$ . The data was de-meanned by subtracting out the mean value over the time series for that given pixel, Equation 4. A zero pad was added to make the series an even power of two ( $N=16$ ). Next a sine window was applied to mitigate spectral leakage, Equation 5. The Fast Fourier Transform (FFT) of the discretely sampled finite record length time series was taken for each pixel within the study area. The spectral density of each pixel was calculated and then averaged over the entire study area using Equations 6-7. By averaging the data it limited the effects of localized events and due to the small record length (16 seconds) it was necessary to filter out as much noise as possible.

$$i_{\text{demean}}(\theta, r, t) = i(\theta, r, t) - \text{mean}(i(\theta, r)) \quad (\text{Equation 4})$$

$i_{\text{demean}}(\theta, r, t)$  = De-meanned Intensity at point  $(\theta, r)$  for each step in time (1:15)

$i(\theta, r, 1:15)$  = Intensity at point  $(\theta, r)$  for each step in time (1:15)

$\text{mean}(i(\theta, r))$  = Mean Intensity for a given point  $(\theta, r)$  over time

$$i_{\text{sine}}(\theta, r, 1:16) = i_{\text{demean}}(\theta, r, 1:16) * \sin(\pi * 1:16/16) \quad (\text{Equation 5})$$

$i_{\text{sine}}(\theta, r, 1:16)$  = Intensity at point ( $\theta, r$ ) for each step in time (1:16) after sine window  
 $i_{\text{demean}}(\theta, r, t)$  = De-meanned Intensity at point ( $\theta, r$ ) for each step in time (1:16)  
 $\sin(\pi * 0:15/15)$  = Sine window for each time step (1:16)

$$\Phi(\theta, r, f) = 2 * N * \Delta t * F(\theta, r) * F^*(\theta, r) \quad (\text{Equation 6})$$

$\Phi(\theta, r, f)$  = Spectral Energy at point ( $\theta, r$ ) for frequency ( $f$ )  
 $N$  = Length of Time Series, 16  
 $\Delta t$  = Time Step of time series, 1 sec  
 $F(\theta, r)$  = Continuous Fourier Transform at point ( $\theta, r$ )  
 $F^*(\theta, r)$  = Complex Conjugate at point ( $\theta, r$ )

$$\Phi_{\text{avg}}(f) = \sum_r \sum_{\theta} \Phi(\theta, r, f) / [(\theta_{\text{max}} - \theta_{\text{min}}) * (r_{\text{max}} - r_{\text{min}})] \quad (\text{Equation 7})$$

$\Phi_{\text{avg}}(f)$  = Average Spectral Energy for the study area at frequency ( $f$ )  
 $\sum_r \sum_{\theta} \Phi(\theta, r, f)$  = Sum of Spectral Energy for all points ( $\theta, r$ ) at frequency ( $f$ )  
 $[(\theta_{\text{max}} - \theta_{\text{min}}) * (r_{\text{max}} - r_{\text{min}})]$  = Area of study area in pixels

The average period observed for each hour was solved for using Equations 8-9. The average period used for comparison was taken from the published NOAA data at Buoy 46050 at the start of a new hour. It is important to note that the buoy average period is taken 15 minutes prior to the radar data at 20 nautical miles to the west.

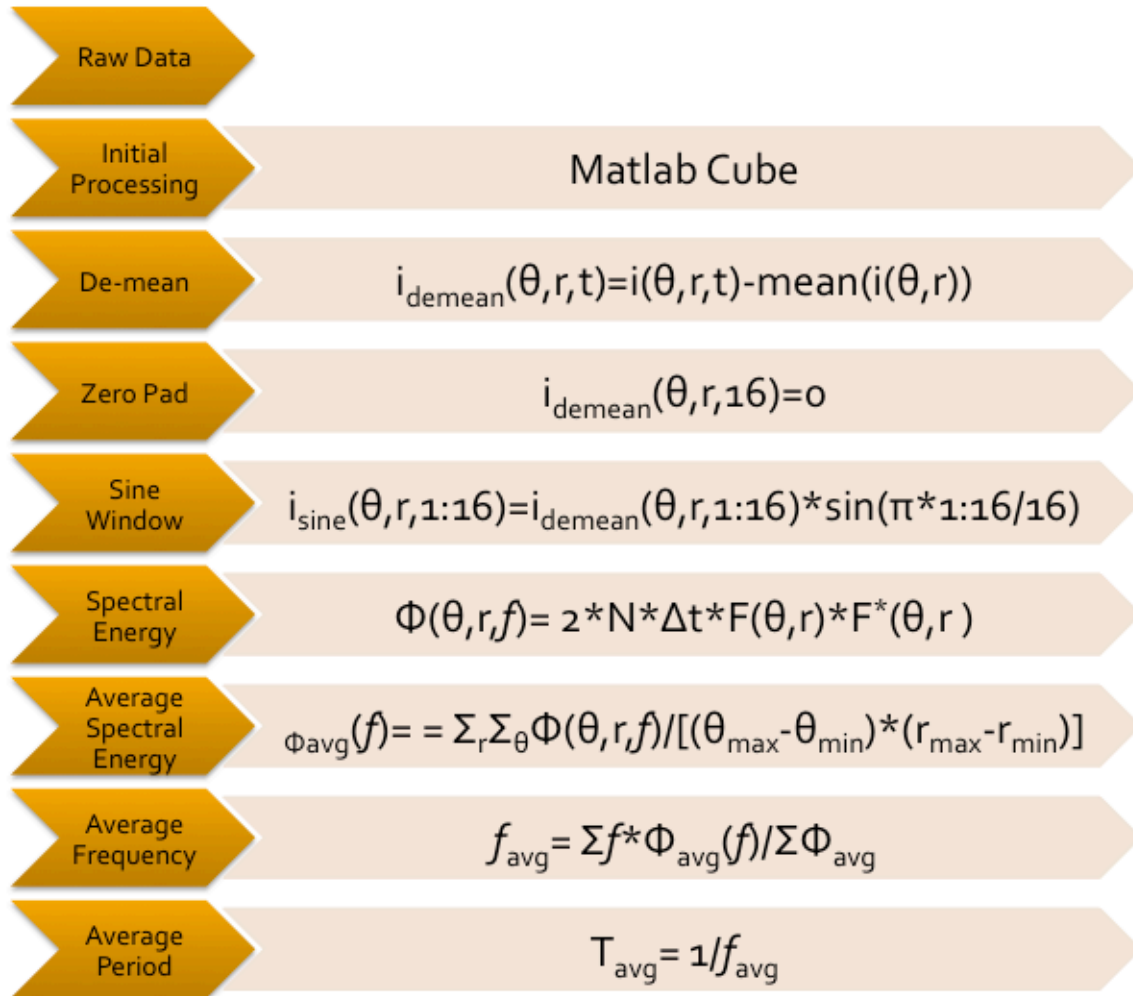
$$f_{\text{avg}} = \sum f * \Phi_{\text{avg}}(f) / \sum \Phi_{\text{avg}} \quad (\text{Equation 8})$$

$f_{\text{avg}}$  = Average Frequency  
 $\sum f * \Phi_{\text{avg}}(f)$  = Sum of Average Spectral Density multiplied by the corresponding frequency  
 $\sum \Phi_{\text{avg}}$  = Sum of Average Spectral Density for all frequencies

$$T_{\text{avg}} = 1 / f_{\text{avg}} \quad (\text{Equation 9})$$

$T_{\text{avg}}$  = Average Period  
 $f_{\text{avg}}$  = Average Frequency

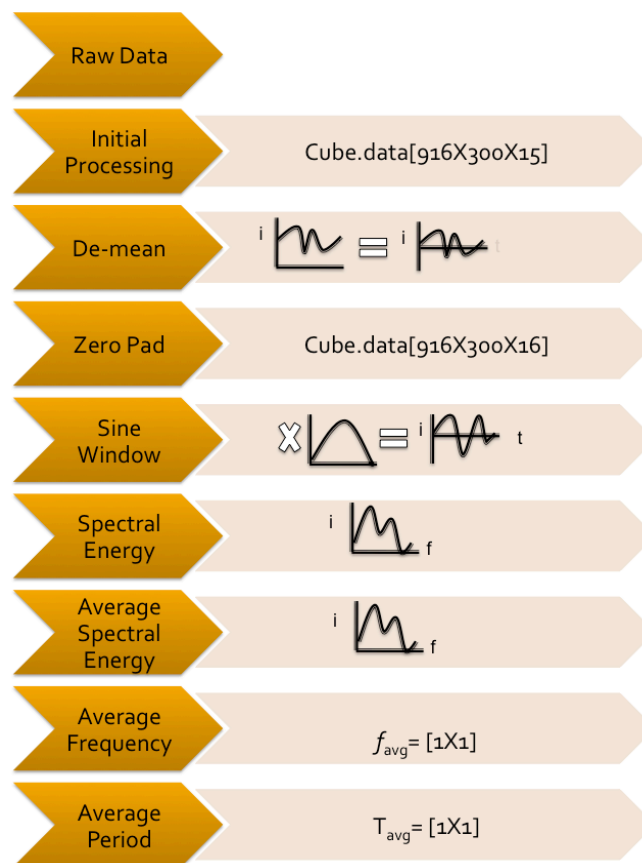
Figure 12 displays a flow chart of the process described above. The steps are listed on the left and the required processing is shown on the right.



**Figure 12: Newport Beach Processing Flow Chart**

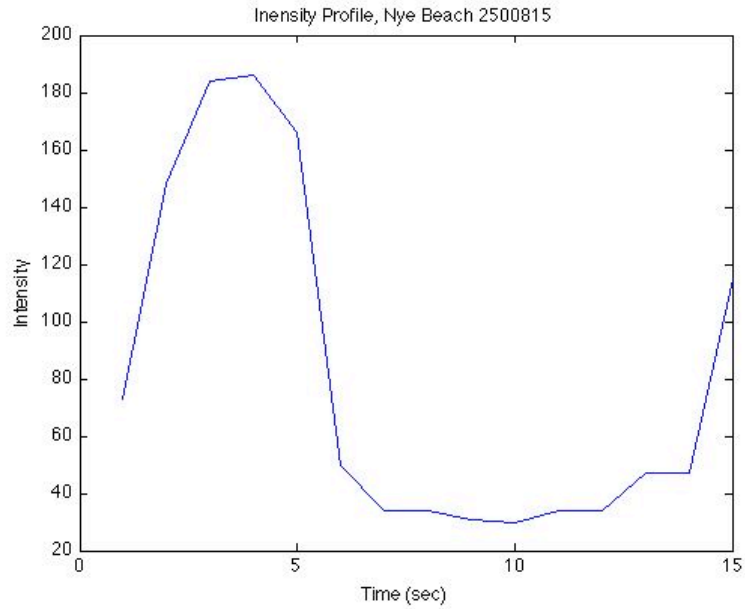
## 4.4 Results -- Newport Beach Study

The results of the data processing are shown in Figure 13 for each step of the Nye Beach and South Beach process. As discussed earlier, the observation lengths were limited to approximately 15 seconds therefore it is expected that the resulting energy spectrum would be coarsely resolved. By de-meaning the data the intensity now fluctuates about zero instead of the mean value. The zero padding step increases the 3-D Cube.data matrix to [916x300x16]. The sine taper reduces the low frequency noise due to the short record length. The spectral energy shows the energy at each frequency. The average energy from the entire study area makes up the average spectral energy. By taking the energy-weighted average of the frequencies, the average frequency for the entire observation series is resolved. The resulting average period for the entire observation series is the inverse of the average frequency.



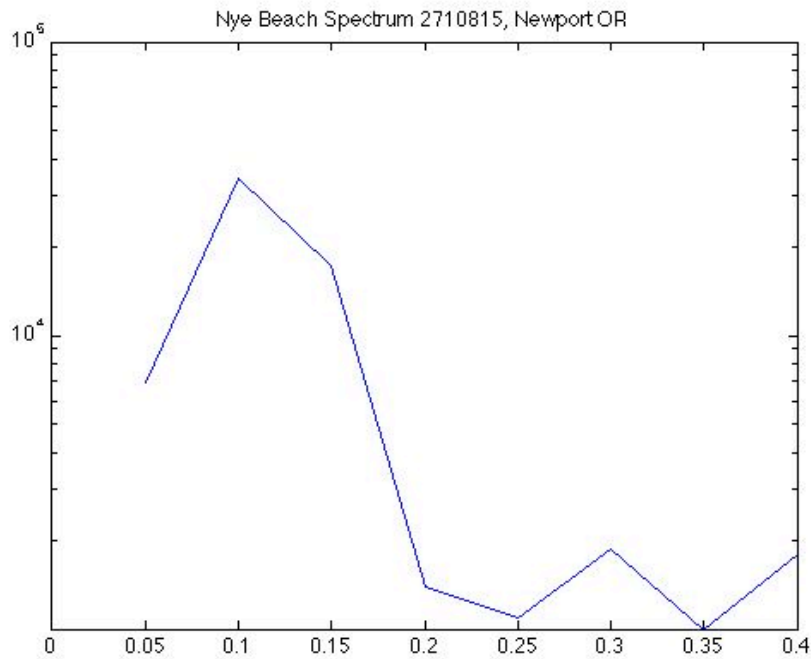
**Figure 13: Newport Beach Results Flow Chart**

An example of the radar intensity time series for a single pixel is shown in Figure 14.



**Figure 14: Example Nye Beach Intensity Time Series**

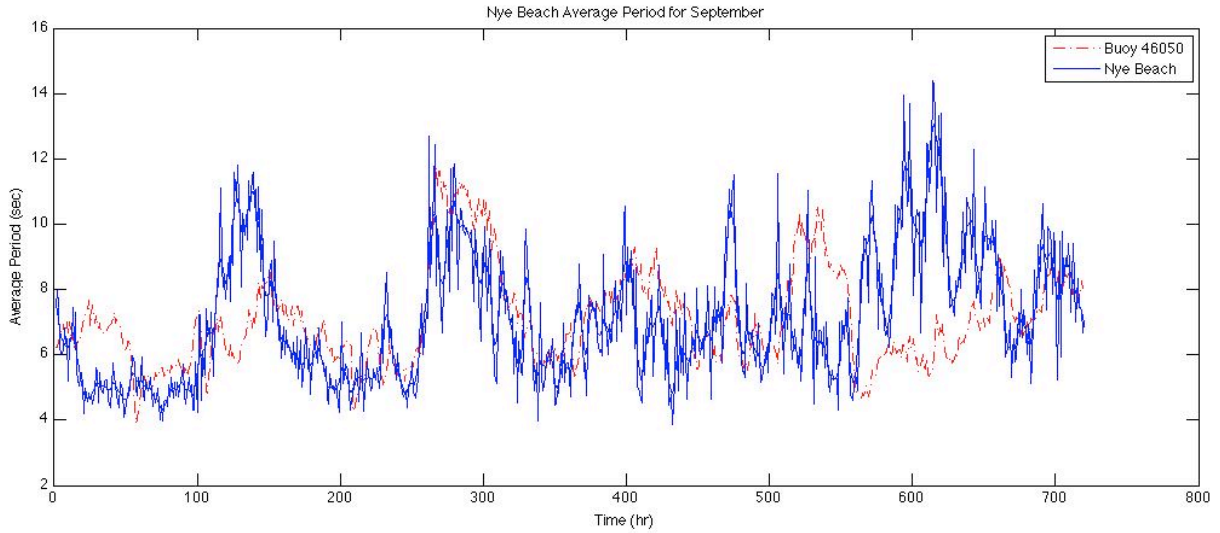
An example of the resulting wave spectrum is shown in Figure 15 where the energy density is a unitless intensity. The spectrum is coarse, as expected, but still shows a dominant energy peak.



**Figure 15: Example Nye Beach Energy Spectrum**

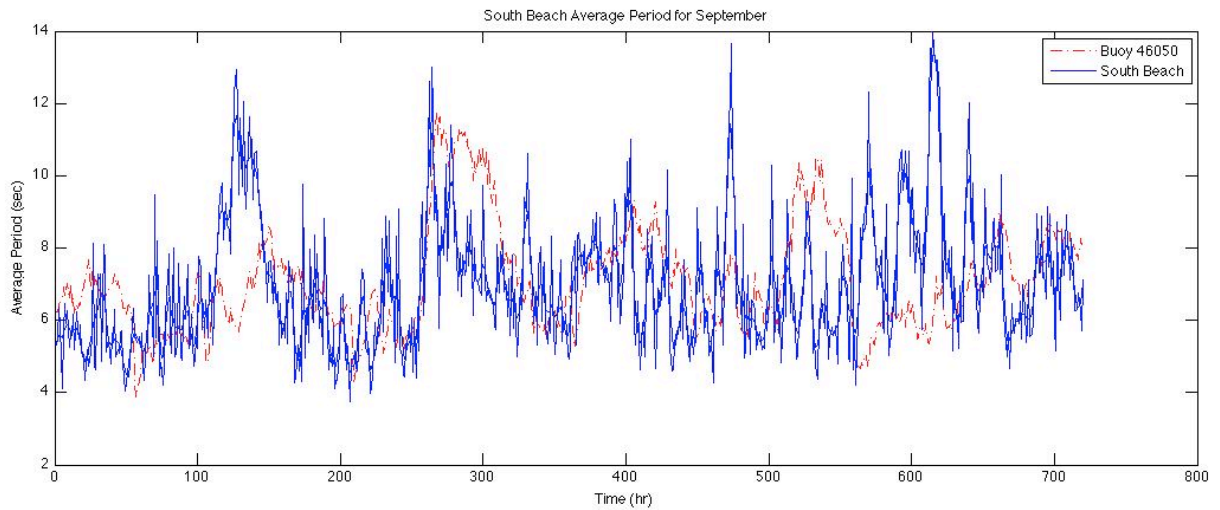


Figure 16 shows a portion of the radar-derived average wave period time series compared to the average period from NDBC 46050. The x-axis shows hours starting with the first hour of the first day of the month. This data is from the Nye Beach study area during the month of September.



**Figure 16 September Nye Beach Average Period**

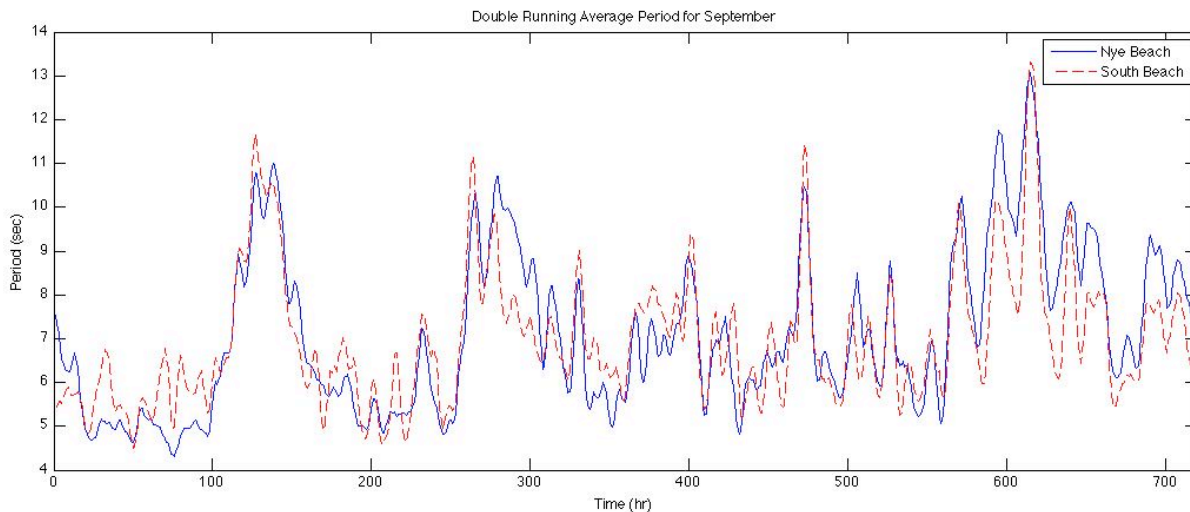
The results for September at the South Beach study area are shown in Figure 17.



**Figure 17 September South Beach Average Period**

## 4.5 Analysis – Newport Beach Study

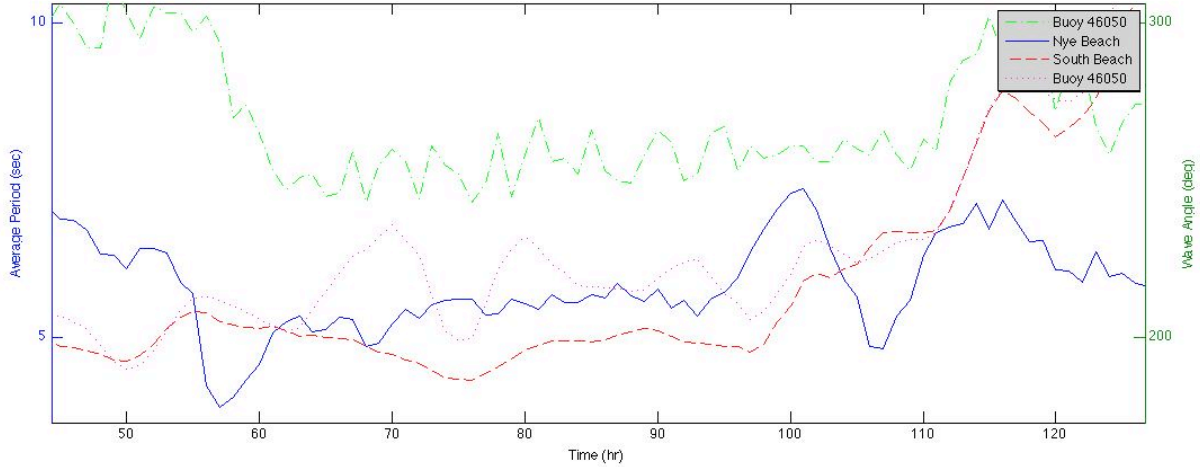
The short record lengths used would allow short-term phenomenon, such as ships passing, to significantly impact the results. Therefore a 4-hour double running average was performed on the radar results to reduce the noise in the signal. This is appropriate since the purpose of this study is to observe the variations induced by tidal effects. The resulting double running average for the month of September at Nye Beach and South Beach are shown in Figure 18. The filtered wave period will be used in the analysis for the rest of this report.



**Figure 18 September Nye and South Beach Double Running Average Period**

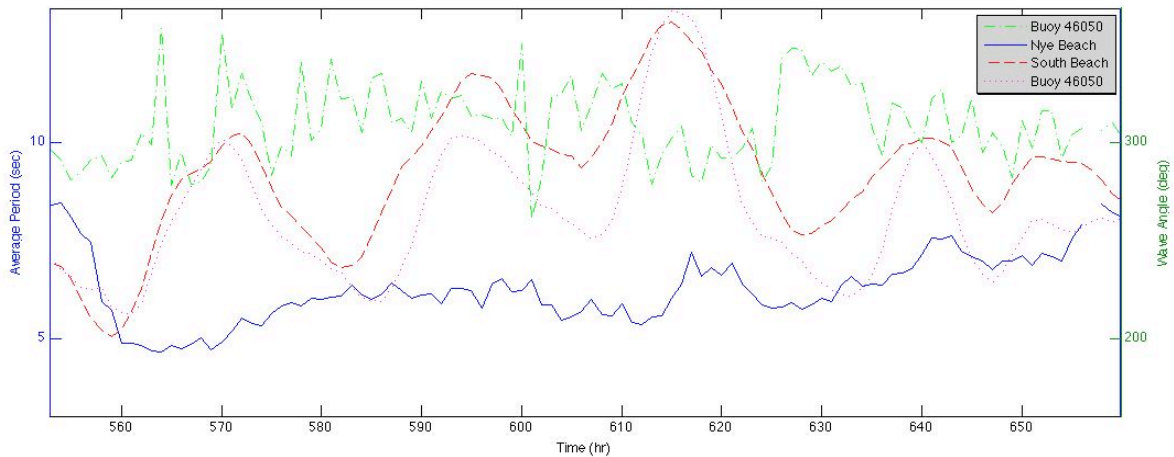
To further investigate some of the differences between the observed average periods at the offshore buoy and those from the shore-based radar we looked at the effects of wave direction. The wave angle of NDBC 46050 is recorded in degrees clockwise from North. It would be expected that as the wave angle shifts toward more oblique direction from shore-normal, the influence of the Jetty would cause differences between South Beach and Nye Beach.

Figure 19 displays a typical trend in which the average period for both Nye Beach and South Beach are close to Buoy 46050 at wave angles of 270 degrees or less. A 270-degree wind angle would mean the wave is coming from the west directly.



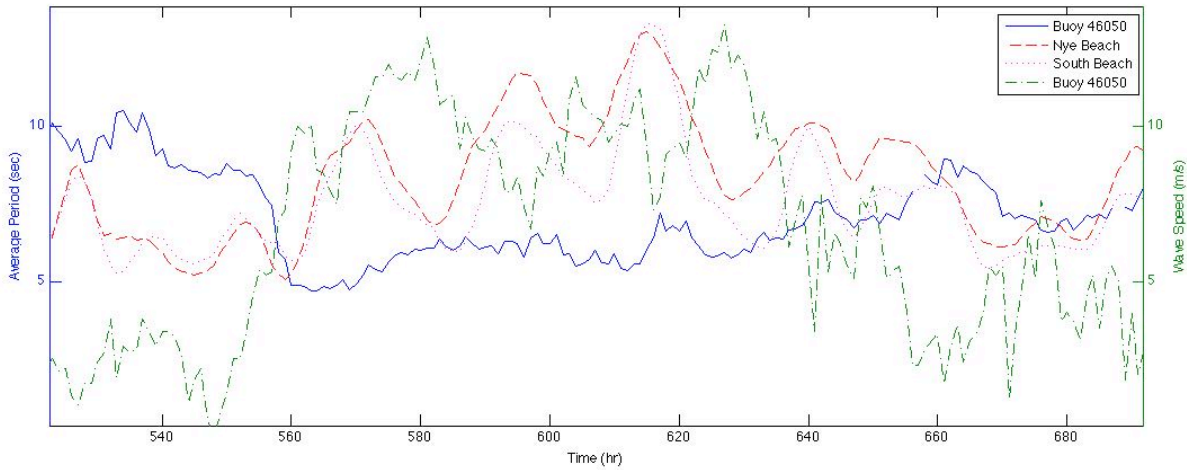
**Figure 19 Nye and South Beach Average Period at Low Wave Angles**

Figure 20 shows the relationship between the Nye and South Beach average period to the Buoy 46050 at higher wind angles. At the higher wind angle the relationship between Nye and South beach are still relatively similar to each other, yet both have a distinct difference to that of Buoy 46050.



**Figure 20 Nye and South Beach Average Period at High Wave Angles**

To further investigate this relationship, Figure 21 shows the same average period data compared at high wind speed recorded at Buoy 46050. At high wind speeds the average period of both Nye and South Beach are significantly larger than that of Buoy 46050 offshore. This is contrary to what is expected by the dispersion relation in which the wave period remains constant during shoaling. Figure 22 shows this relationship of similar average wave periods at low wind speeds.



**Figure 21 Nye and South Beach Average Period at High Winds Speeds**

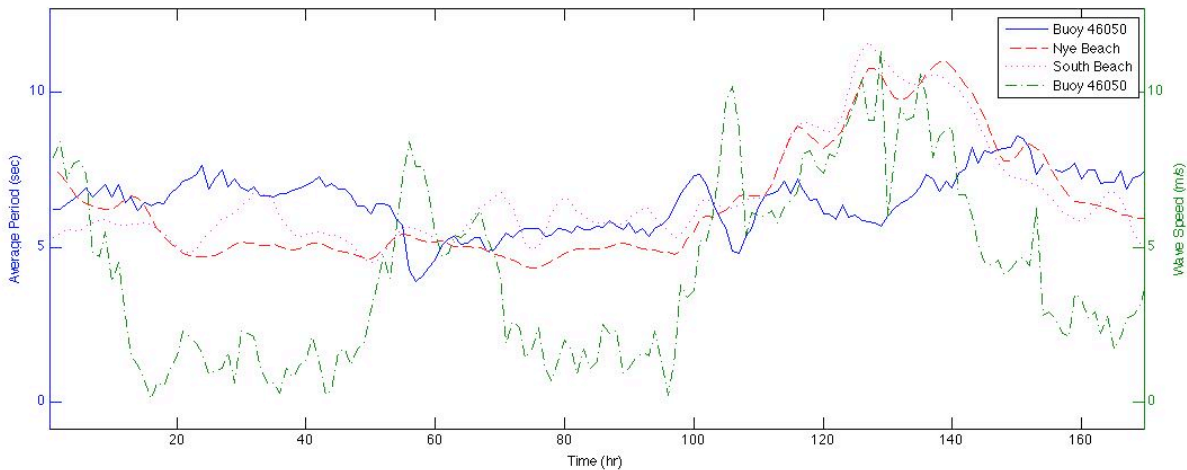


**Figure 22 Nye and South Beach Average Period at Low Winds Speeds**

Figure 23 displays a radar image during the series shown in Figure 21. More wave activity is clearly seen during high wind speeds in Figure 23 as compared to low wind speeds in Figure 24.

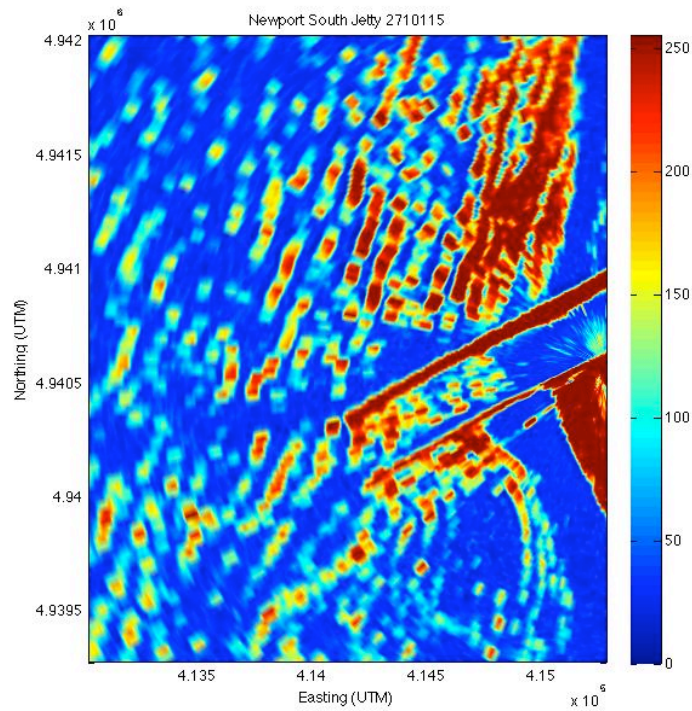


**Figure 23 Radar Image at High Wind Speeds**

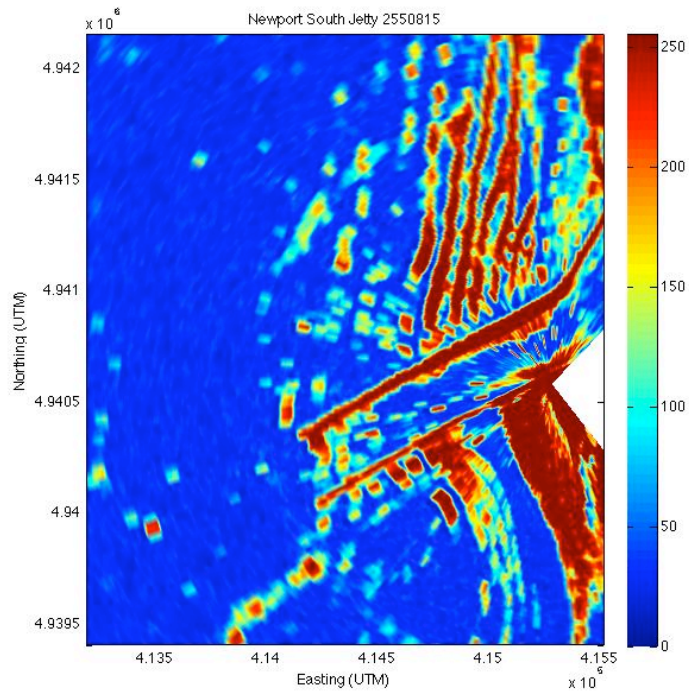


**Figure 24 Radar Image at Low Wind Speeds**

Figure 25 and 26 are the resulting wave energy spectra from the low wind speed conditions. Figure 25 uses the original study area where Figure 26 uses an alternate study area directly adjacent. It is clear that the wave energy spectra are similar in shape and would correspond to a similar average period. This verifies that the average period results found during low wind speeds are a true representation of the wave conditions.

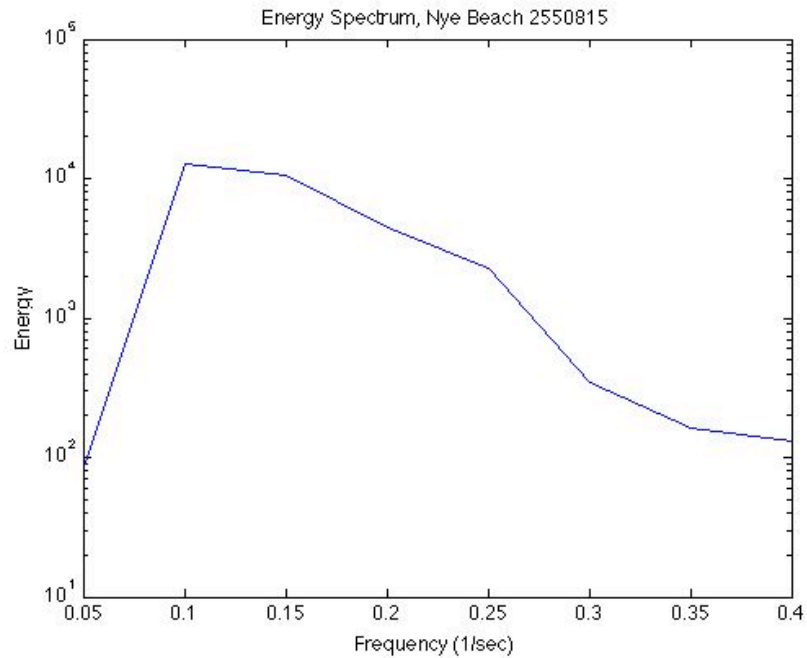


**Figure 25 Wave Energy Spectrum at Low Wind Speeds (Original Study Area)**

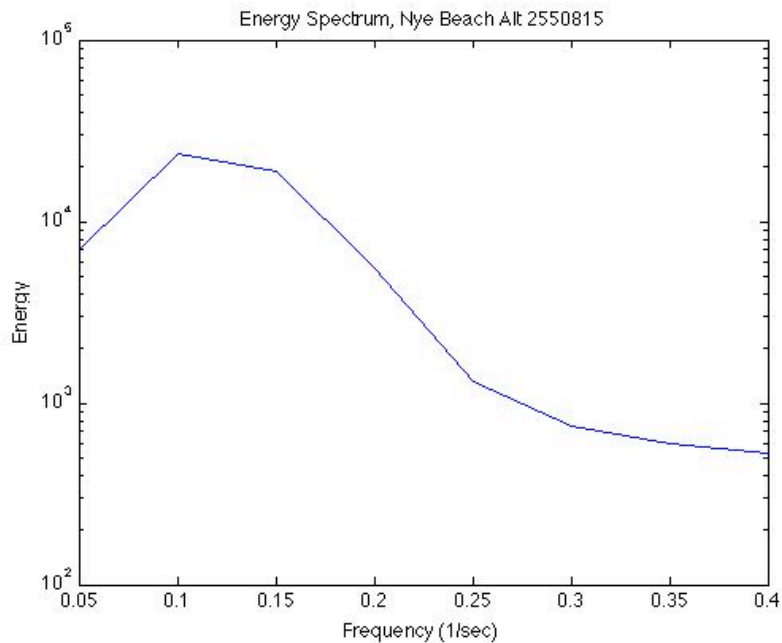


**Figure 26 Wave Energy Spectrum at Low Wind Speeds (Alternate Study Area)**

Figure 27 and 28 are resulting wave energy spectra from the high wind speed conditions. Figure 27 is from the Nye Beach study area that resulted in an average period of 10.25 seconds or a frequency of 0.0975 (1/sec). Figure 28 is from the South Beach study area that resulted in an average period of 7.607 or a frequency of 0.1315 (1/sec). The dominant average periods are well represented by the shape of their wave energy spectra. Therefore the changes observed in wave period as a result of high wind speed change are valid.

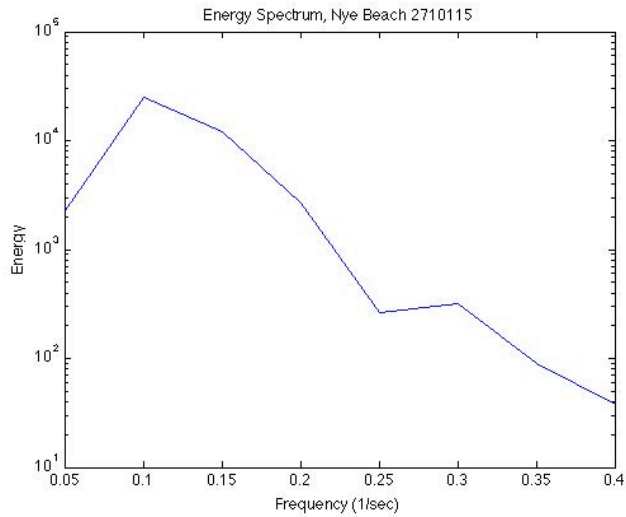


**Figure 27 Nye Beach Wave Energy Spectrum at High Wind Speeds**

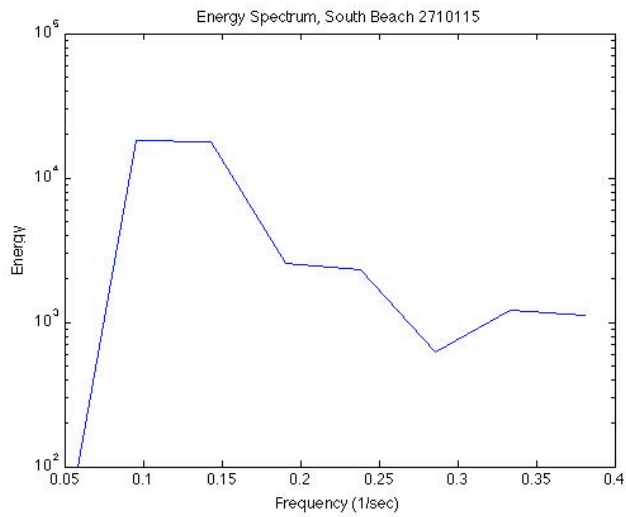


**Figure 28 South Beach Wave Energy Spectrum at High Wind Speeds**

## 4.6 Data Processing -- Newport Jetty Study

In the second portion of the Newport study the jetty mouth was isolated as seen in Figure 29.

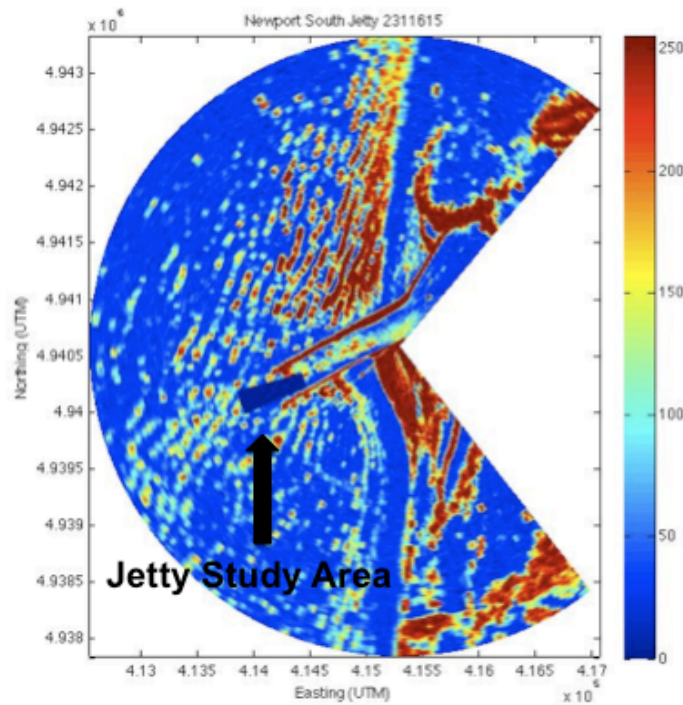


Figure 29 Jetty Study Area

The purpose of this study is to observe the effects of wave steepening or current effects at the Jetty mouth. The intensities recorded at each pixel were averaged for each collection using Equation 10. Then this average was taken over the subset study area. The result represents the mean intensity observed in the area and is normalized by the maximum possible intensity (256) and then given as a percent. A result of 100% would represent a mean intensity of 256 observed over the entire area. This measure of wave activity will be compared to the average variance to examine the coherence to tidal currents. The processing diagram is shown in Figure 11.

$$i_{\text{mean-pixel}}(\Phi, r) = \Sigma i(\Phi, r) / N \quad (\text{Equation 10})$$

$i_{\text{mean-pixel}}(\Phi, r)$  = Mean Intensity for each pixel ( $\Phi, r$ )

$\Sigma i(\Phi, r)$  = Sum of Intensities at pixel ( $\Phi, r$ ) for all time steps  $t=1:15$

$N$  = Number of time steps, 15

$$i_{\text{mean}} = \Sigma_{\theta} \Sigma_r i_{\text{mean-pixel}}(\Phi, r) / [(\theta_{\text{max}} - \theta_{\text{min}}) * (r_{\text{max}} - r_{\text{min}}) * 256] * 100\% \quad (\text{Equation 11})$$

$i_{\text{mean}}$  = Mean Intensity of the study area as a percent

$i_{\text{mean-pixel}}(\Phi, r)$  = Mean Intensity for each pixel ( $\Phi, r$ )

$[(\theta_{\text{max}} - \theta_{\text{min}}) * (r_{\text{max}} - r_{\text{min}})]$  = Area of study area pixels



Variance was calculated using Equation 12 for each point in the polar coordinates. The variance was then averaged over the entire study area, Equation 13. The tidal data that will be compared was taken from verified Mean Lower Low Water (MLLW) NOAA recordings at Station 9435380. MLLW is “the average of the lower low water height of each tidal day observed over the National Tidal Datum Epoch” (NOAA).

$$\sigma^2(\theta,r)=\Sigma(i(\theta,r,1:16)-\text{mean}(i(\theta,r)))^2 \quad \text{(Equation 12)}$$

$\sigma^2(\theta,r)$ = Variance at point  $(\theta,r)$

$i(\theta,r,1:16)$ = Intensity at point  $(\theta,r)$  for each time step (1:16)

$\text{mean}(i(\theta,r))$ = Mean Intensity for a given point  $(\theta,r)$  over time

$$\sigma^2_{\text{avg}}=\Sigma\sigma^2(\theta,r)/[(\theta_{\text{max}}-\theta_{\text{min}})*(r_{\text{max}}-r_{\text{min}})] \quad \text{(Equation 13)}$$

$\sigma^2_{\text{avg}}$ = Average Variance

$\sigma^2(\theta,r)$ = Variance at point  $(\theta,r)$

$[(\theta_{\text{max}}-\theta_{\text{min}})*(r_{\text{max}}-r_{\text{min}})]$ = Area of study area pixels

#### 4.7 Results – Newport Jetty Study

The data processing flowchart is shown in Figure 30 for the Jetty study. Calculation of Mean Intensity results in one value representing the hourly observation. Likewise, the variance is averaged over the study area returning one variance value representing the hourly observation.

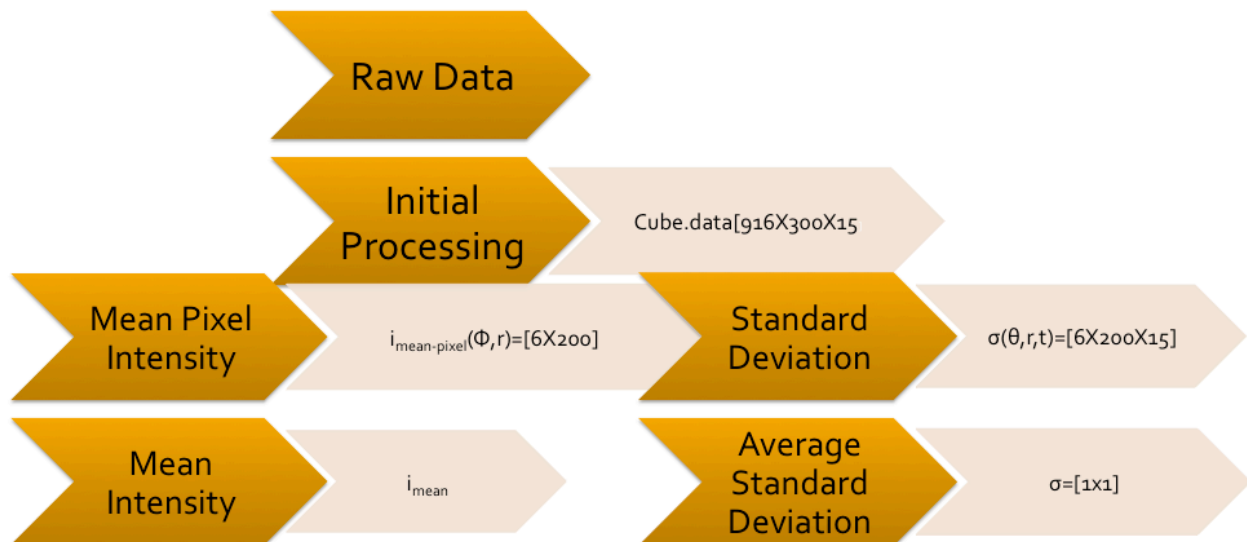
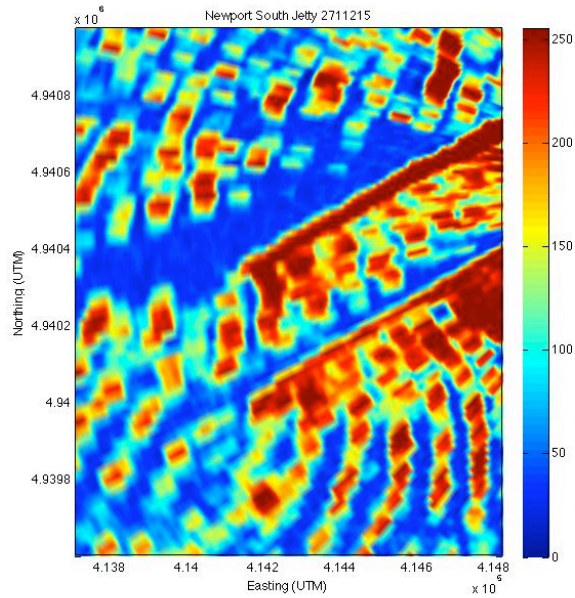
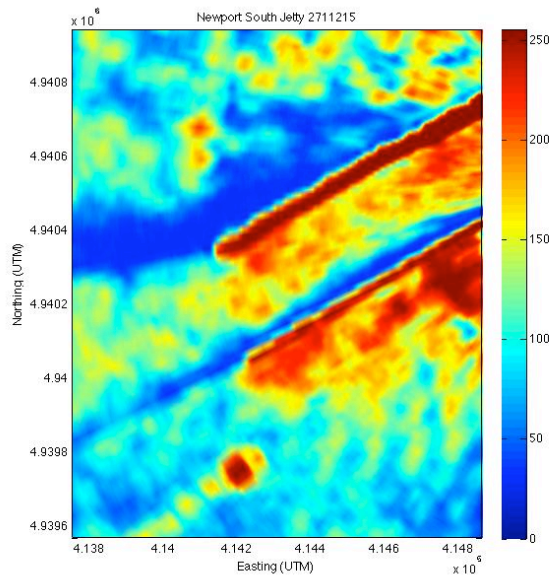


Figure 30 Jetty Data Processing Flow Chart

Figure 31 displays an example of a single radar image at the Jetty mouth. The individual waves are identifiable. Figure 32 displays the mean intensity where the individual waves cannot be seen. The areas of high mean intensity represent the pixel locations where high intensities are consistently seen. This can be interpreted as the area of frequency breaking waves

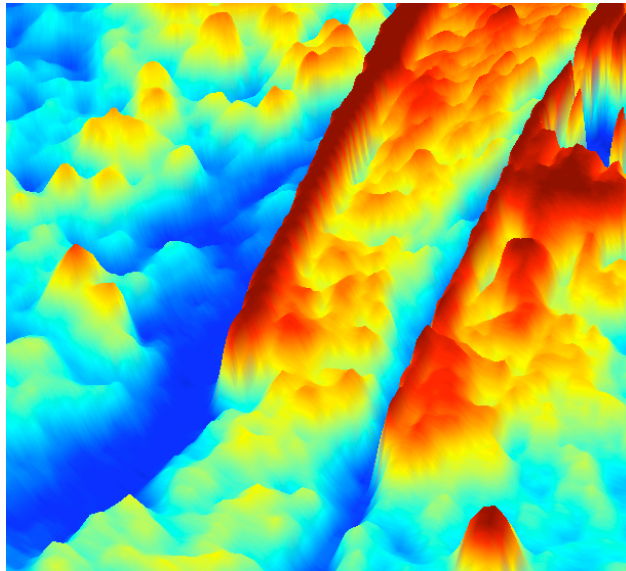


**Figure 31 Jetty Radar Image**



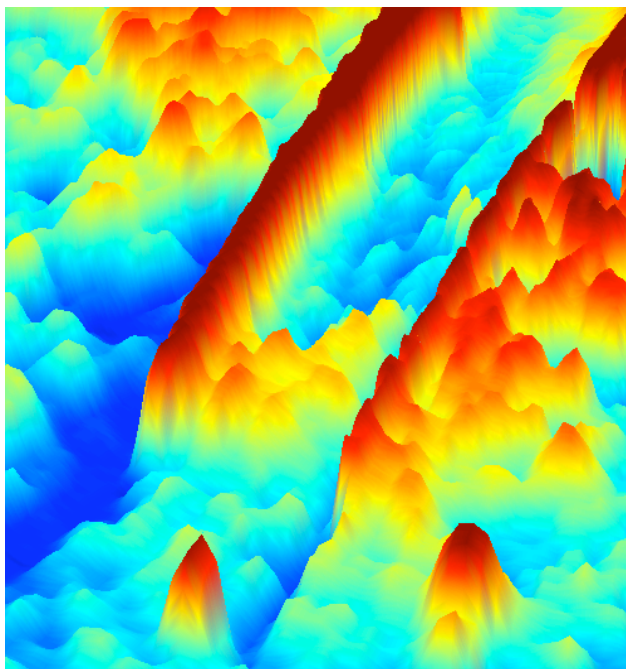
**Figure 32 Jetty Mean Intensity Image**

It is expected that during times of heavy wave breaking the mean intensity will be larger in area and intensity. This can be seen in the 3-D image of the jetty mouth in Figure 33.



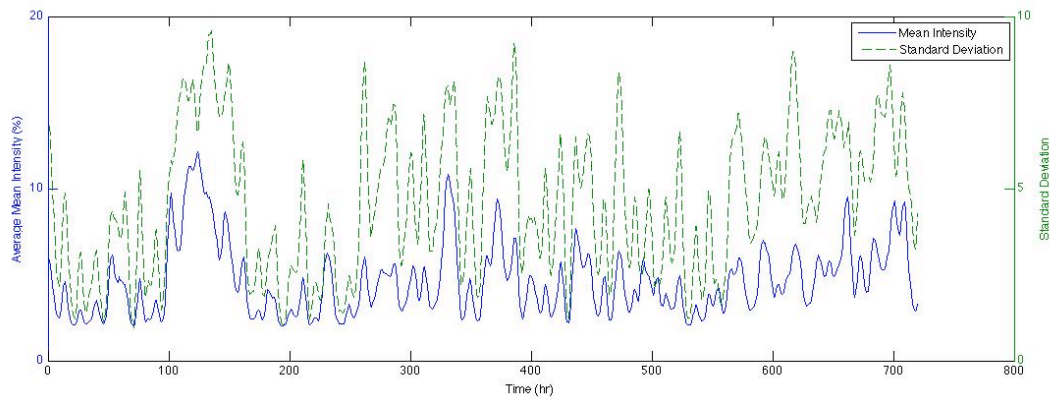
**Figure 33 Jetty Heavy Wave Breaking**

The Mean Intensity shown in this figure shows that the wave breaking area fills the jetty mouth. Whereas in Figure 34 the wave breaking area fills only a portion of the jetty mouth during minimal wave action.



**Figure 34 Jetty Minimal Wave Breaking**

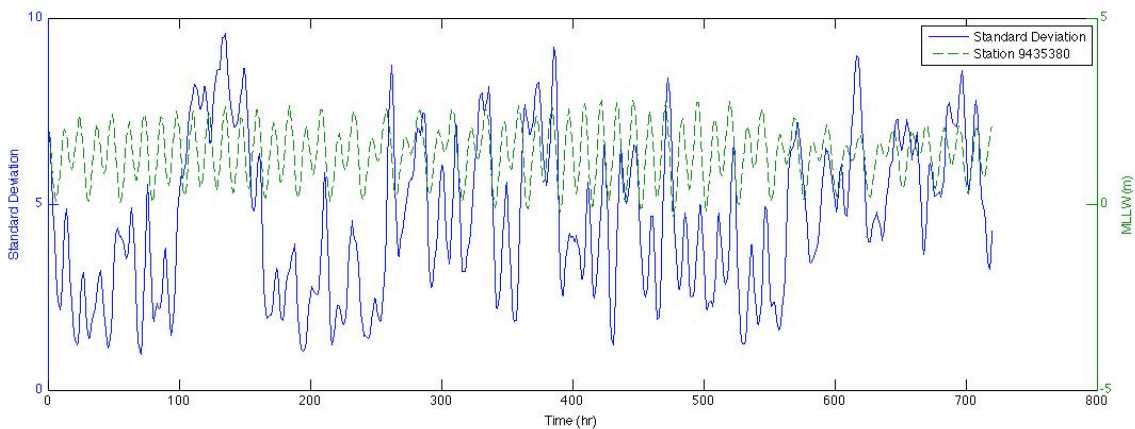
The factors causing the change in breaking area will be discussed in 4.8 Analysis-Jetty Study. Also to be analyzed is the factors contributing to changes in the standard deviation results. Figure 35 shows the results of the Mean Intensity and Average Standard Deviation calculations for each hourly observation in the month of September. The time measure on the x-axis is in hours starting with the first hour of the first day of the month.



**Figure 35 Jetty Mean Intensity and Average Standard Deviation**

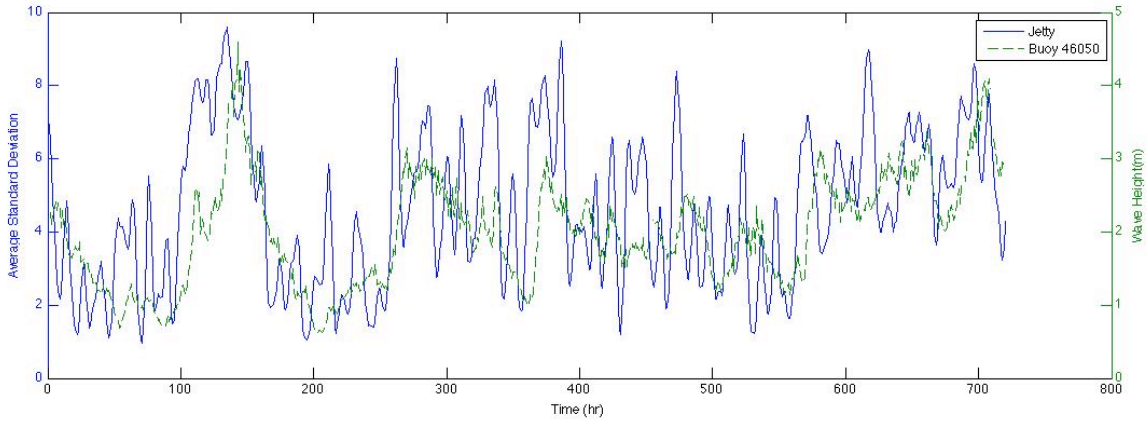
#### 4.8 Analysis – Newport Jetty Study

In order to analyze the patterns observed at the Jetty mouth Figure 36 plots the Average Standard Deviation and Tide together. It is apparent that the slight fluctuation in tidal signal does not accurately describe the abrupt changes in Standard Deviation.



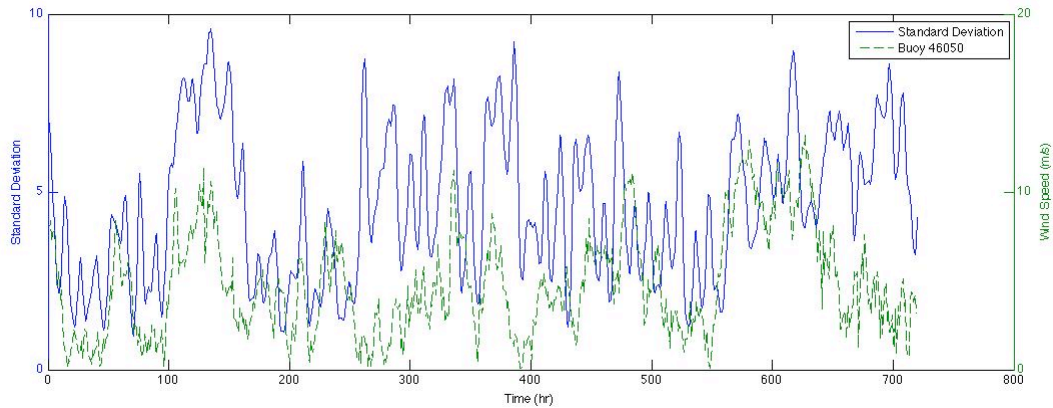
**Figure 36 Jetty Average Standard Deviation vs Tide (MLLW)**

By plotting Average Standard Deviation and Wave Height in Figure 37 the changes are significantly correlated.



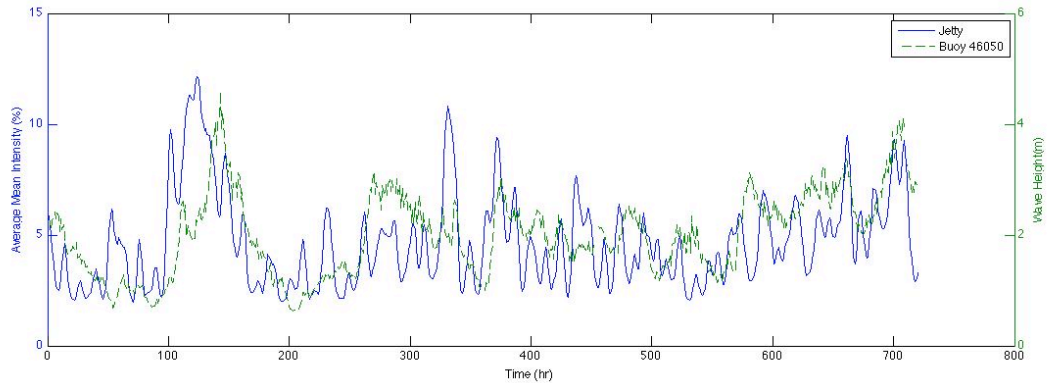
**Figure 37 Jetty Average Standard Deviation vs Wave Height**

Figure 38 plots Average Standard Deviation and Wind Speed, which are also correlated but not as tightly as Wave Height. This is due to the fact that higher wind speeds generate higher waves. But as the wind speed dies off the wave height will lag and depend on other factors such as fetch.



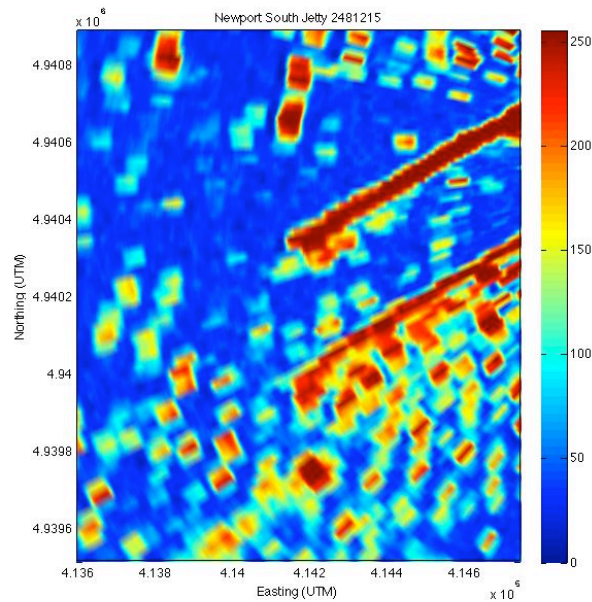
**Figure 38 Jetty Average Standard Deviation vs Wind Speed**

Figure 39 plots the Average Mean Intensity with Wave Height. This shows a similar correlation to the Average Standard Deviation in which Wave Height appears to be the driving factor. The Average Mean Intensity increases, which means the area of wave breaking increases with Wave Height.



**Figure 39 Jetty Average Mean Intensity vs Wave Height**

Figure 40 and 41 display the radar image and resulting mean intensity during the low wave heights of the series shown in Figure 39.



**Figure 40 Jetty Image at Low Wave Heights**

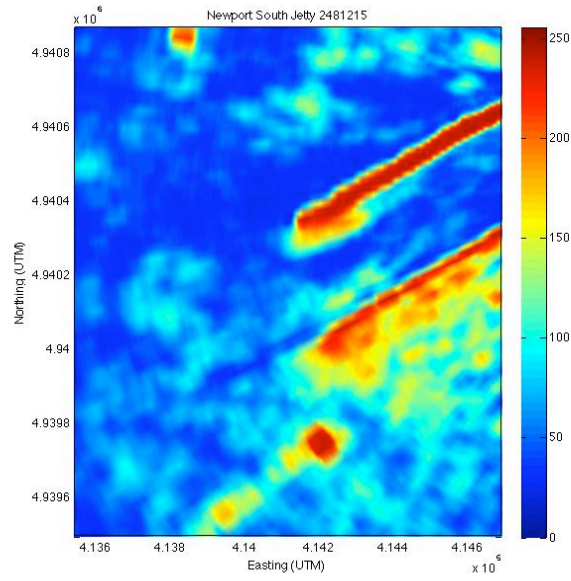


**Figure 41 Jetty Mean Intensity at Low Wave Heights**

Figures 42 and 43 show the radar image and resulting mean intensity during the high wave heights. There are clearly more waves seen in the Jetty and the area of breaking is expanded compared to the low wave heights in Figures 40 and 41.

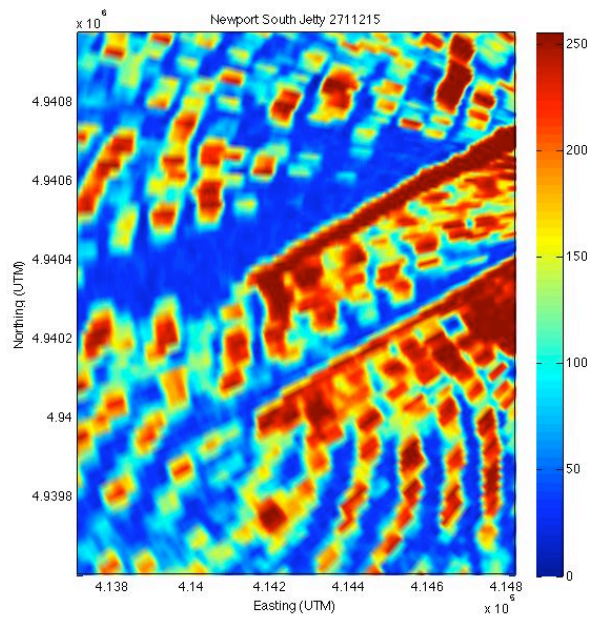


**Figure 42 Jetty Image at High Wave Heights**

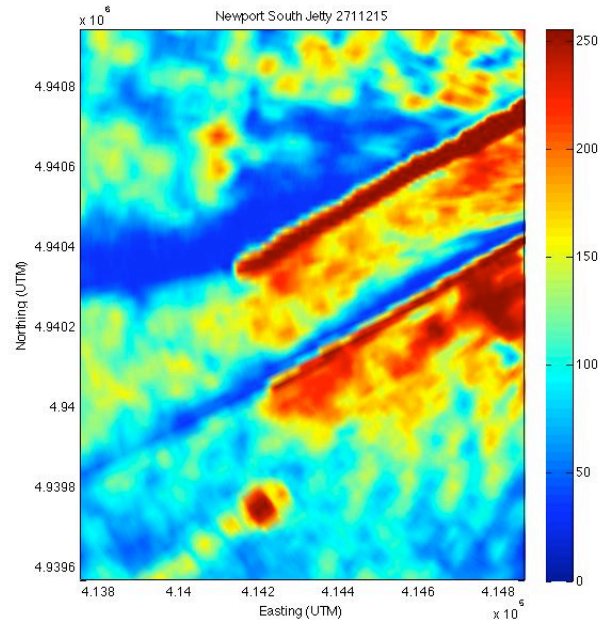


**Figure 43 Jetty Mean Intensity at High Wave Heights**



## 5 Shipboard Observations -- Reedsport

The Reedsport Study will be used to establish baseline environmental conditions prior to the installation of a wave energy generation array. The study is funded by the Oregon Wave Energy Trust (OWET) who's mission is to "serve as a connector for all stakeholders involved in wave energy project development - from research and development to early stage community engagement and final deployment and energy generation - positioning Oregon as the North America leader in this nascent industry and delivering its full economic and environmental potential for the state." The radar data used in this study was taken directly from the operating radar of the U.S. charter boat Miss Linda during three deployments. The images were captured while underway using a VGA to USB conversion device and software.

### 5.1 Site Conditions -- Reedsport

Officially incorporated in 1919, the city of Reedsport lies at the mouth of the Umpqua River. Although the area is well known as one of the state's most popular recreational fishing areas, the main attraction for the area is the Oregon Dunes National Recreation Area. In an effort to increase the local economy and in support of OWET's progressive alternative energy efforts, the Reedsport community will be home to a wave energy generation site. Specifically, the initial 14 wave energy buoys will be installed just north of Brushy Hill approximately 1 mile offshore as shown in Figure 44. The PowerBuoy 150 (PB150)

wave energy buoys are manufactured by Ocean Power Technologies (OPT) and are rated at 150 kilowatts each. Wave information for the region is provided by National Oceanic and Atmospheric Administration (NOAA) thru a buoy at Umpqua Offshore Buoy 46229 (43°46'10" N 124°33'2" W), seen in Figure 45.



Figure 44 Reedsport Wave Energy Array Site



**Figure 45 Umpqua Offshore Buoy 46229 Location**

## 5.2 Set Up -- Reedsport

The shipboard radar data was taken during two excursions in which the primary mission was to deploy observation buoys in support of the OWET study. These excursions took place on September 18th and October 8th, 2009. The ship used for the deployment was the U.S. charter boat Miss Linda, shown in Figure 46. The homeport of the Miss Linda is Coos Bay, Oregon and she is captained by Bob Pedro. The radar onboard the Miss Linda uses a 4 kilowatt Furuno radome antenna (Figure 47), providing a maximum range of 36 nautical miles and a 3.9 degree beam width.



**Figure 47 Charter Boat Miss Linda**



**Figure 46 Miss Linda Radar**

The data was recorded directly from the radar display using a VGA2USB device manufactured by Epiphan Systems Inc, shown in Figure 47. The VGA2USB device captures the image directly from the radar screen to a laptop using the VGA2USB software, shown in Figure 48. This differs from the Newport study in which the data was recorded directly from the radar.



Figure 48 VGA2USB



Figure 49 Miss Linda Data Recording

### 5.3 Data Processing -- Reedsport

The raw data was recorded in image (.jpg) files. In order to process the data each image was imported into Matlab. After importing the pixelated image becomes a matrix of [VertXHorizXt] where Vert is the number of pixels in the vertical direction and Horiz is the number of pixels in the horizontal direction and t is the number of time steps in the series. For the Miss Linda data the vertical pixels are 480 and the horizontal pixels are 650 [480X650Xt]. Figure 50 shows an example of the Miss Linda image overlaid on its relative position to Reedsport, OR.

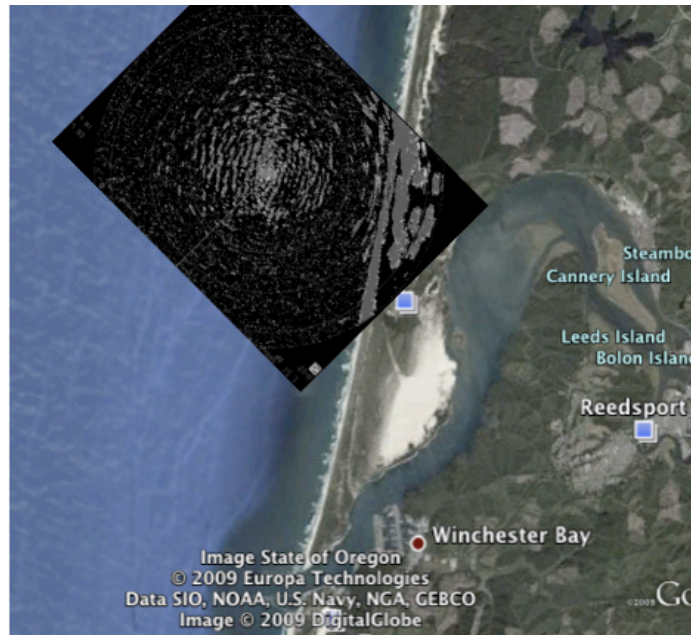
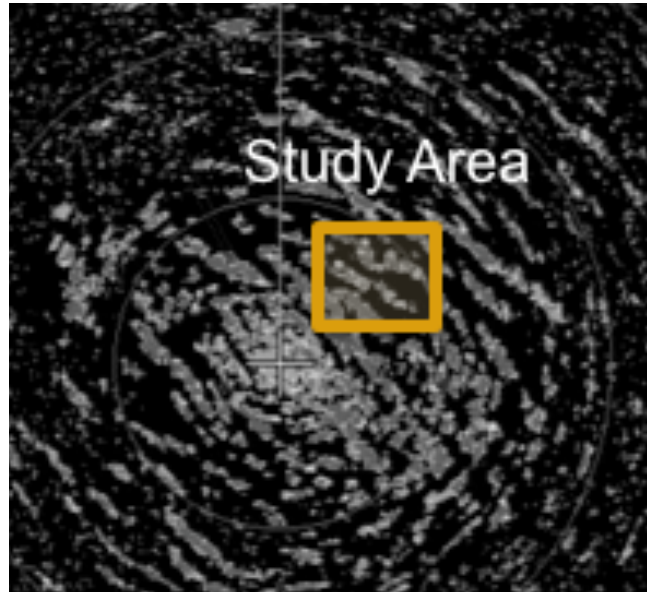


Figure 50 Reedsport Results and Location

The data were processed using similar steps as in the Newport Nye Beach and South Beach Study. The data from September 18<sup>th</sup> was isolated at [200:225,375:400,t] as shown in Figure 51. The length of time series for the series was 771 seconds long at a sampling rate of 0.778 seconds. In order to reduce the effects of ship movement the total series was divided into several 64-second series.



**Figure 51 September Study Area**

The data from October 8<sup>th</sup> was isolated at [225:250,250:275,t] as shown in Figure 52. The length of time series for the series was 766 seconds long at a sampling rate of 0.782 seconds.

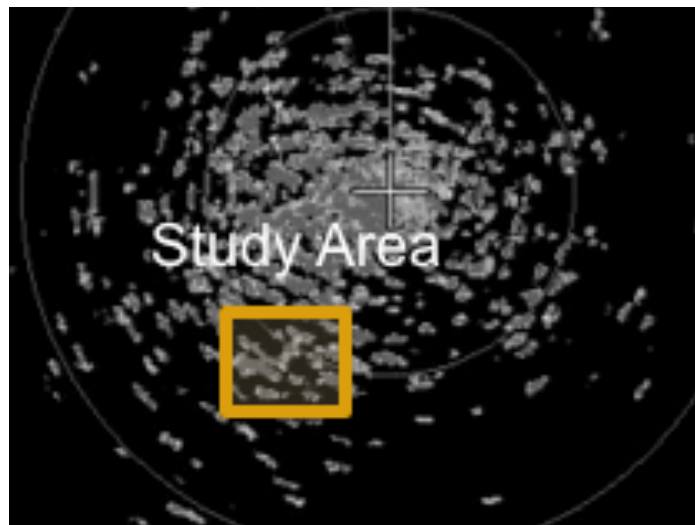


**Figure 52 October Study Area**

The Average Period was calculated using the process described in 4.3 Data Processing-Beach Study. However the zero-padding step was not required. The significantly longer time series than that of the Newport Study now made it possible to calculate wave spectra at a much higher resolution. Therefore, it is also possible to calculate a more precise Peak Period. The Peak Period found simply by identifying the frequency at which the most spectral energy is located and taking it's inverse. The process used to calculate Average and Peak Period for the Reedsport Study is shown in Figure 53.

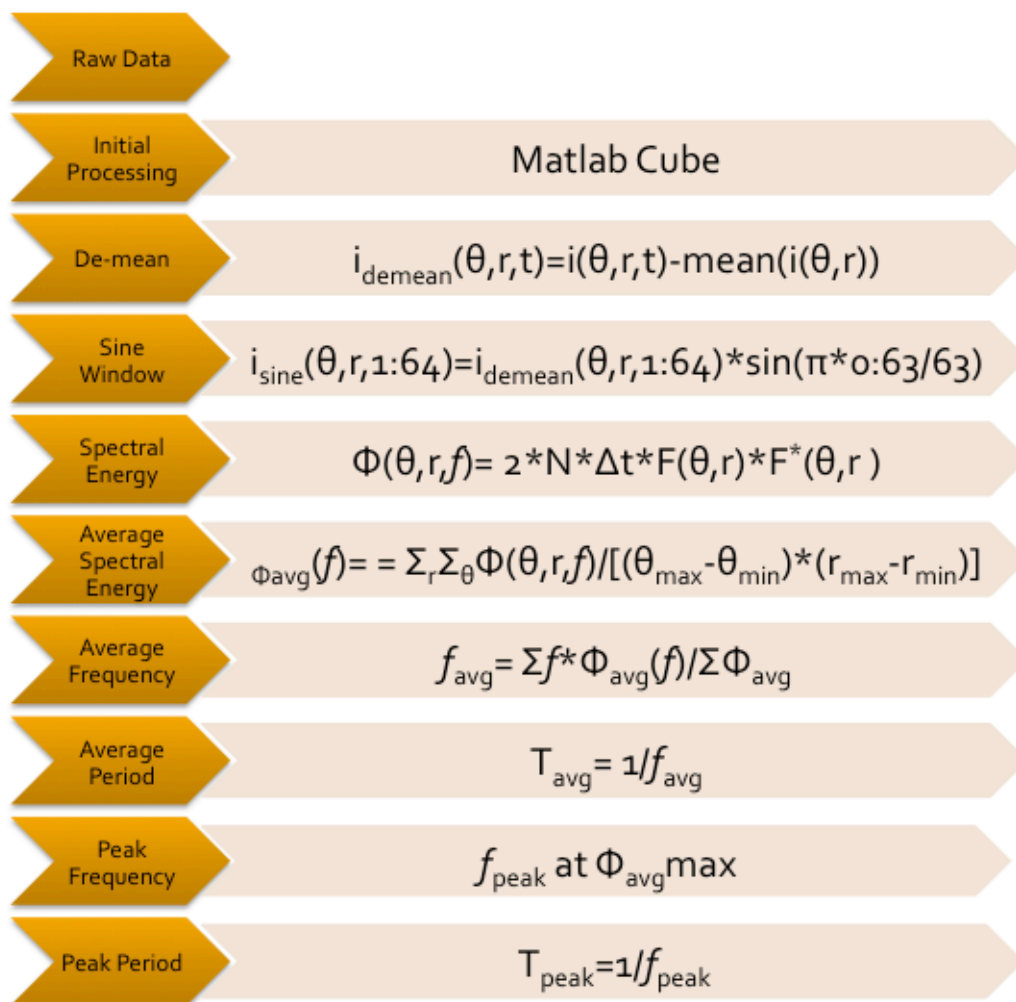


**Figure 53 Reedsport Data Processing Flow Chart**

## 5.4 Results -- Reedsport

The resulting wave energy spectra for the September 18<sup>th</sup> deployment is shown in Figures 54-56.

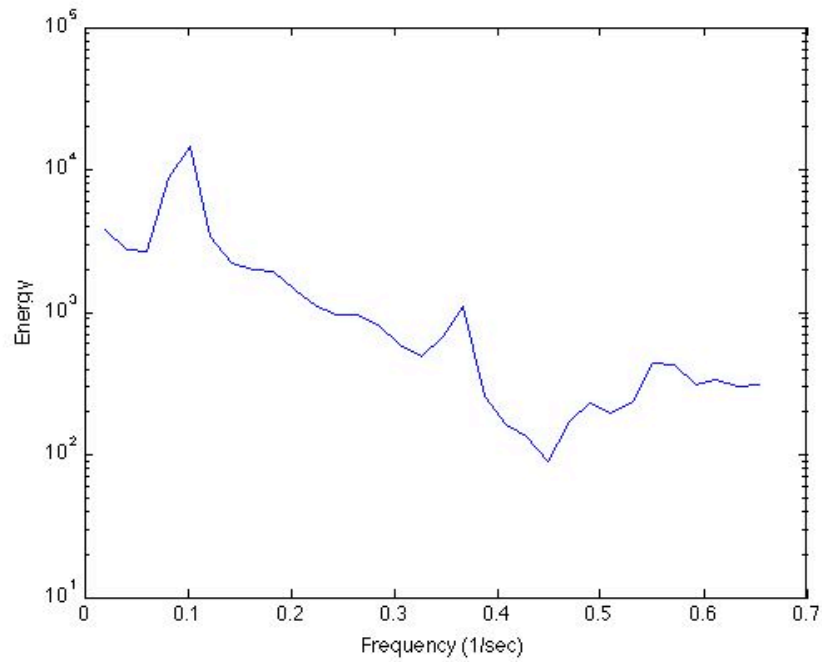


**Figure 54 September Reedsport Wave Energy Spectrum - 1**

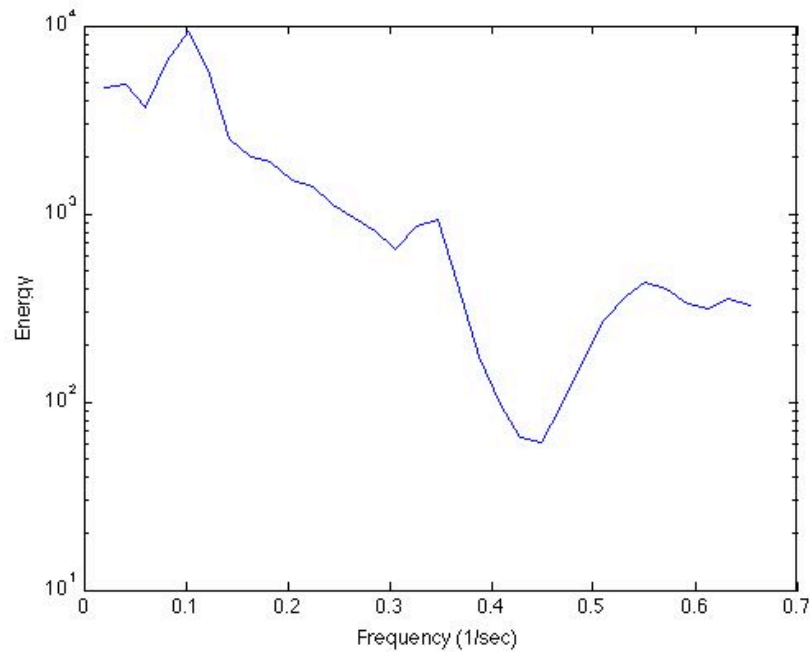


**Figure 55 September Reedsport Wave Energy Spectrum - 2**

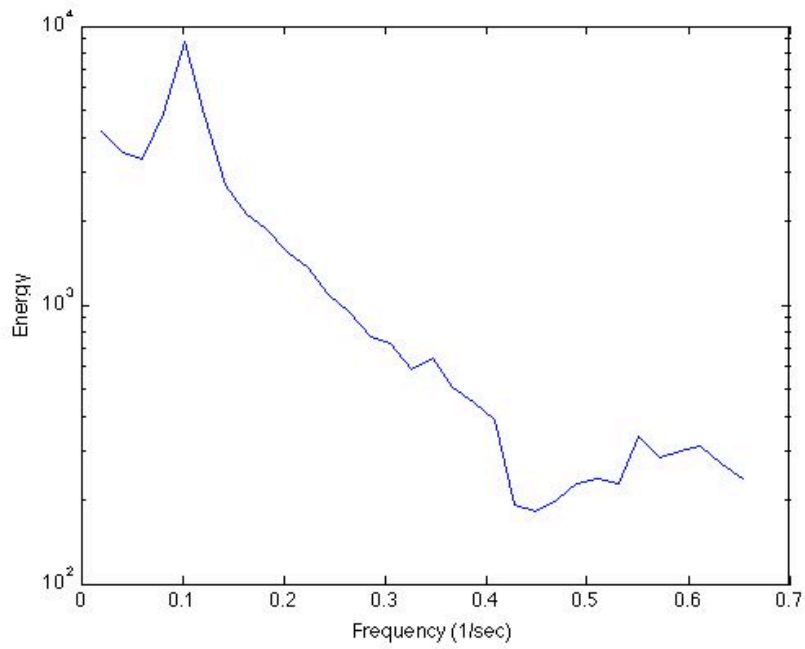


**Figure 56 September Reedsport Wave Energy Spectrum - 3**

The resulting wave energy spectrum for the October 8<sup>th</sup> deployment is shown in Figures 57-59.

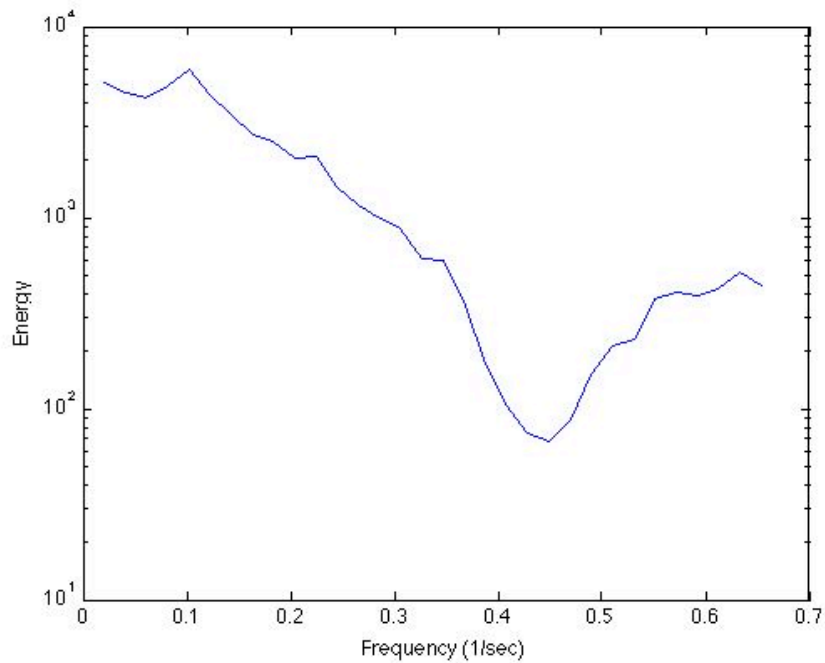


**Figure 57 October Reedsport Wave Energy Spectrum - 1**

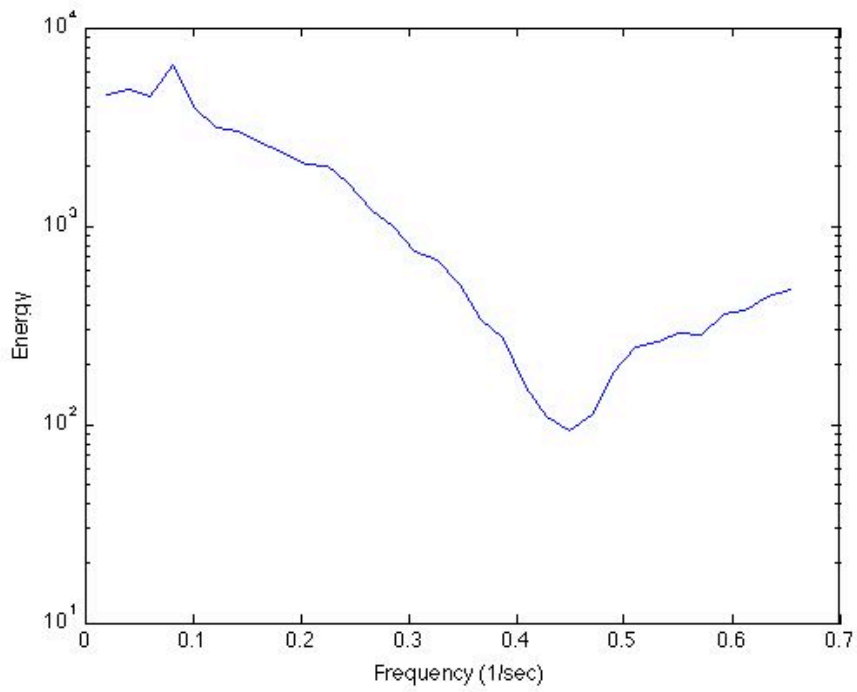


**Figure 58 October Reedsport Wave Energy Spectrum - 2**

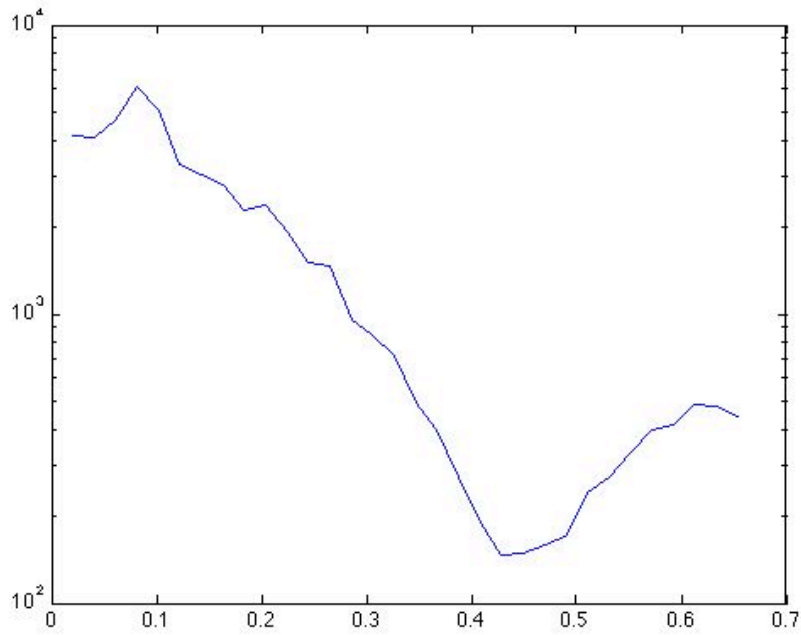


**Figure 59 October Reedsport Wave Energy Spectrum - 3**



## 5.5 Analysis -- Reedsport

The resulting period values of the shipboard radar data and that taken from the wave buoy are compared in Table 2.

**Table 2 Reedsport Results Compared to Buoy 46229**

|                | Peak Period (sec) | Buoy Peak Period | Average Period (sec) | Buoy Average Period (sec) |
|----------------|-------------------|------------------|----------------------|---------------------------|
| September 18th | 9.96              | 9.88             | 8.4                  | 8.23                      |
| October 8th    | 9.79              | 9.88             | 7.5                  | 7.06                      |

It is apparent that the wave periods observed by the Miss Linda shipboard radar accurately represent those recorded by Buoy 46229. This would allow the use of Buoy 46229 to provide initial wave conditions for the OWET wave energy array study. Radar data could then be collected at a nearshore location to record the changes in wave spectrum due to the wave energy array interactions.

## 6 Conclusion

Commercial marine radar technology can be used to collect wave statistics. Either shore-based or shipboard systems are appropriate as long as the radar location remains stationary. Longer record lengths can greatly increase the accuracy of the results.

### 6.1 Shore-Based Station -- Newport

The shore-based station reported key long-term trends for the surrounding nearshore area. The average wave periods observed at Nye and South Beach corresponded well to those seen at Buoy 46050 during low wind speeds. At higher wind speeds the Nye and South Beach period greatly increased as compared to Buoy 46050. This may be due to high-speed wave groups dispersing during the travel between the buoy observation and at Nye and South Beach. It may also be due to other wind generation or wave dissipation processes.

The Average Mean Intensity and Average Standard Deviation at the Jetty showed significant correlation to the Wave Height observations at Buoy 46050. If the Average Standard Deviation was calibrated to in-situ wave height testing, the sea state conditions at the Jetty mouth could

then be estimated using the shore-based radar station. This would provide valuable information to local boaters if broadcasted using the existing network system.

## **6.2 Shipboard Observations -- Reedsport**

The peak and average period observed by the shipboard radar accurately represented those recorded at Buoy 46229. If a similar semi-permanent radar system were installed during the testing of the wave energy array, it would be expected that the results of the wave energy array on the wave spectrum could be observed. Buoy 46229 could be utilized to establish initial wave conditions while nearshore radar would record resulting conditions.

## **6.3 Additional Research**

Preparations are already being made to allow for longer time series observations at the shore-based Newport radar site. A time series of  $N \geq 60$  is recommended. With these longer time series the full wave spectrum would be more accurately represented. Wave angle and wavelength could then be calculated using cross-spectral analysis. The wave intensities can also be calibrated to provide accurate wave height estimates as shown in (Holland, 1997).

A nearshore system should be calibrated with in-situ testing at the Reedsport wave energy array site. This would allow for accurate wave spectrum measurement over the immediate area. Observations could then be made on the effects of wave interaction within the array as well as on the surrounding nearshore.

## 7 References

- City of Reedsport*. GOV office.com, 2007. Web. <<http://www.reedsport.or.us/>>. 04 Oct. 2009.
- Discover Newport, "Newport Oregon and the Central Oregon Coast - History." *Newport Oregon and the Central Oregon Coast - Home*. Web. <<http://discovernewport.com/index.php/about/history>>. 07 Dec. 2009.
- Holland, K.T, R.A. Holman, T.C. Lippmann, J. Stanley and N. Plant. Practical use of video imagery in nearshore oceanographic field studies. *IEEE Journal of Oceanic Engineering* (special issue on image processing for oceanic applications), 22(1), 81–92, 1997.
- Integrated Publishing, "Range Resolution." *Aerographer and Meteorology Training Manuals*. Web. <[http://www.tpub.com/content/aerographer/14271/css/14271\\_62.htm](http://www.tpub.com/content/aerographer/14271/css/14271_62.htm)>. 10 Oct. 2009.
- National Oceanic and Atmospheric Administration, "Mean Lower Low Water (MLLW)." *NOAA Tides and Currents*. Web. <<http://tidesandcurrents.noaa.gov/mlw.html>>. 04 Nov. 2009.
- Northwest Research Associates, Inc, "Coastal Video Monitoring Station." *Video Metric Systems*. <<http://www.planetargus.com/stades.html>>. Aug. 2001. Web. 07 Dec. 2009.
- Oregon Wave Energy Trust*. Web. . <http://www.oregonwave.org/>, 2009 24 Oct. 2009
- State Coastal Conservancy, *California Coastal Currents Monitoring Program*. Los Angeles: Print, 2009.
- Terrill, Eric J. "Mapping Surface Currents Around the U.S." *Sea Technology*. UCSD, Sept. 2007. Web. 15 Oct. 2009. <[http://cordc.ucsd.edu/projects/mapping/documents/2007\\_Terrill\\_HFRNet.pdf](http://cordc.ucsd.edu/projects/mapping/documents/2007_Terrill_HFRNet.pdf)>.
- Traenkmann, Ina. "Waves and currents by X-band radar." *Coastal Wiki*. Flanders Marine Institute, Sept. 2008. Web. <[http://www.coastalwiki.org/coastalwiki/Waves\\_and\\_currents\\_by\\_X-band\\_radar](http://www.coastalwiki.org/coastalwiki/Waves_and_currents_by_X-band_radar)>. 07 Oct. 2009.
- U.S. Marine Corps, *Field Antenna Handbook*. MCRP 6-22D. Quantico: Print, 1999.
- Varshney, Lav. *Radar System Components and Design*. Tech. 1st ed. North Syracuse: Syracuse Research Corporation, 2002.
- Ward, Donald L. *Case Histories of Corps Breakwater and Jetty Structures*. Tech. Vol. 6. Vicksburg: Coastal Engineering Research Center, Department of the Army, 1988.

Wolf, Christian. "The Radar Equation." *Radar Tutorial*. SELEX, Nov. 2008. Web.  
<<http://www.radartutorial.eu/01.basics/rb13.en.html>>. 17 Nov. 2009.

## 8.1 Guy Wire Design

The equation used to calculate wind force is shown in Equation #.

$$F = A * P * C_d \quad (\text{Equation \#})$$

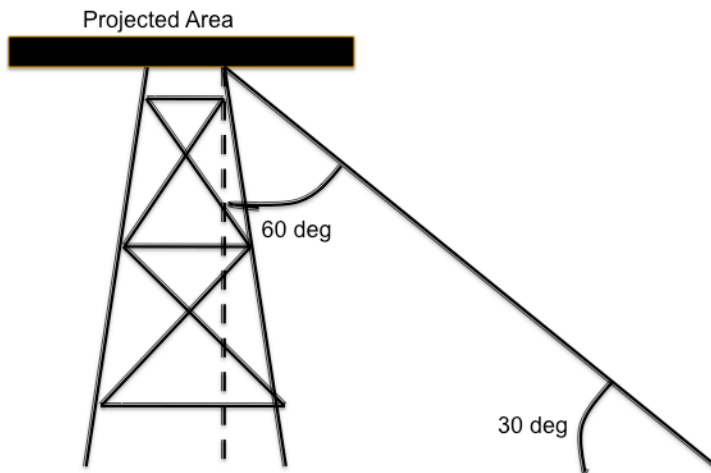
$F =$  Force (lbs)  
 $A =$  Project Area (ft<sup>2</sup>)  
 $P =$  Wind Pressure (Psf)  
 $C_d =$  Drag Coefficient

Wind pressure can be estimated using Equation #. The drag coefficient of 1.2 is used for an ideal long cylinder (antenna tube).

$$P = 0.00256 * V^2 \quad (\text{Equation \#})$$

$P =$  Wind Pressure (Psf)  
 $V =$  Wind Speed (mph)

As seen in Figure # the required axial tension capacity can be calculated by enforcing the wind force at the top of the tower. For simplicity, the guy wire system will be designed as if all the loading was on one wire. An additional wire will be installed for each corner during construction for redundancy. Table # displays the resulting required load capacities.



|                                   |        |
|-----------------------------------|--------|
| Max Wind Speed (mph)              | 150    |
| Wind Pressure (Psf)               | 57.6   |
| Projected Area (ft <sup>2</sup> ) | 4      |
| Drag Coefficient                  | 1.2    |
| Force (lb)                        | 276.48 |
| Factor of Safety                  | 5      |
| Min Capacity x (lb)               | 1382   |
| Min Capacity y (lb)               | 421    |
| Min Capacity axial (lb)           | 1445   |

## 8.2 Matlab Script

```
%Information for processing individual Months
W=['May', 'Jun', 'Jul', 'Aug', 'Sep'];
X=['05', '06', '07', '08', '09'];
Y=[31 30 31 31 30];
Z=[1210015 1520015 1820015 2130015 2440015];

%Required Input, rfile is starting file name
Month='Jul';
MO='07';
Days=31;
sfile=1820015

%Load master file
load Period.mat;
load Intense.mat;
load Dev.mat

%Process first hour
addpath(['\\lennon\scratch\haller-shipops\SouthJetty\2009-07-'
num2str(01, '%02.0f')])
tfile=sfile;
hours=[0:23];
numfiles=24;
i=1;
%j is hour
for j=1:numfiles
    fname=tfile
    %Process raw data into Cube

[Cube]=ReadSouthJettyBin(fname,[415281.912896239,4940576.5966031
23,57,85,14.144],1,1,1);
    warning off;

    %Conduct Nye Beach Study
    %Set dimensions of study area, d=deg of theta, r=pixel
radius
    dmn=350;
    dmx=450;
    rmn=165;
    rmx=205;
    %Establish parameters for FFT
    N=16;
    dt=60/(Cube.results.TrueRPM);
    df=1/(dt*N);
```

```

freq=[df:df:N*df/2];
A.avg=zeros(16,1);
count=0;
for d=dmn:dmx
    for r=rmn:rmx
        count=count+1;
        A.raw=double(squeeze(Cube.data(d,r,:)));
        %De-mean
        A.raw=A.raw-mean(A.raw);
        %Zero-pad
        A.raw(16)=0;
        %Sine Window
        A.sin=A.raw.*sin(pi*[0:15]'/15);
        %FFT
        A.fast=fft(A.sin)./N;
        %Spectral Energy
        A.energy=2*abs(A.fast).^2/df;
        %Sum Energy for Average Fr
        A.avg=A.avg+A.energy;
    end
end
%Solve Average Energy
A.avg=A.avg/count;
%Solve Average Frequency (1-sided)
A.avf(j)=sum(freq'.*A.avg(2:9))/sum(A.avg(2:9));
%Solve Average Period
A.avT(j)= 1./A.avf(j);

%Conduct South Beach Study
%Set dimensions of study area
dmn2=250;
dmx2=400;
rmn2=100;
rmx2=117;
B.avg=zeros(16,1);
count=0;
for d=dmn2:dmx2
    for r=rmn2:rmx2
        count=count+1;
        B.raw=double(squeeze(Cube.data(d,r,:)));
        %De-mean
        B.raw=B.raw-mean(B.raw);
        %Zero-pad
        B.raw(16)=0;
        %Sine Window
        B.sin=B.raw.*sin(pi*[0:15]'/15);
        %FFT
        B.fast=fft(B.sin)./N;
    end
end

```

```

        %Spectral Energy
        B.energy=2*abs(B.fast).^2/df;
        %Sum Energy for Average Fr
        B.avg=B.avg+B.energy;
    end
end
%Solve Average Energy
B.avg=B.avg/count;
%Solve Average Frequency (1-sided)
B.avf(j)=sum(freq'.*B.avg(2:9))/sum(B.avg(2:9));
%Solve Average Period
B.avT(j)= 1./B.avf(j);

%Conduct Jetty Study
%Set dimensions of study area
dmn3=300;
dmx3=500;
rmn3=122;
rmx3=128;
C.tot=0;
C.st=0;
for r=rmn3:rmx3
    for d=dmn3:dmx3
        %Sum up total radar intensity
        C.tot=C.tot+sum(double(squeeze(Cube.data(d,r,1:15))));
        %Sum std dev for pixel
        C.st=C.st+std(double(squeeze(Cube.data(d,r,1:15))),1);
    end
end
%Mean radar intensity (%) over study area x 15 time steps
C.int(j)=C.tot/((dmx3-dmn3)*(rmx3-rmn3)*15)*100;
%Average std dev over study area
C.dev(j)=C.st/((dmx3-dmn3)*(rmx3-rmn3));

%Start next file
tfile=tfile+100;
end
Period.Nye.(Month)=A.avT';
Period.South.(Month)=B.avT';
Intense.Jetty.(Month)=C.int';
Dev.Jetty.(Month)=C.dev';

%Cycle for rest of month
for i=2:Days
    sfile=sfile+10000;
    addpath(['\\lennon\scratch\haller-shipops\SouthJetty\2009-

```



```

07-' num2str(i, '%02.0f']]
    tfile=sfile;
    hours=[0:23];
    numfiles=24;
    %j is hour
    for j=1:numfiles
        fname=tfile
        %Process raw data into Cube

[Cube]=ReadSouthJettyBin(fname,[415281.912896239,4940576.5966031
23,57,85,14.144],1,1,1);
        warning off;

        %Conduct Nye Beach Study
        %Set dimensions of study area, d=deg of theta, r=pixel
radius
        dmn=350;
        dmx=450;
        rmn=165;
        rmx=205;
        %Establish parameters for FFT
        N=16;
        dt=60/(Cube.results.TrueRPM);
        df=1/(dt*N);
        freq=[df:df:N*df/2];
        A.avg=zeros(16,1);
        count=0;
        for d=dmn:dmx
            for r=rmn:rmx
                count=count+1;
                A.raw=double(squeeze(Cube.data(d,r,:)));
                %De-mean
                A.raw=A.raw-mean(A.raw);
                %Zero-pad
                A.raw(16)=0;
                %Sine Window
                A.sin=A.raw.*sin(pi*[0:15]'/15);
                %FFT
                A.fast=fft(A.sin)./N;
                %Spectral Energy
                A.energy=2*abs(A.fast).^2/df;
                %Sum Energy for Average Fr
                A.avg=A.avg+A.energy;
            end
        end
        %Solve Average Energy
        A.avg=A.avg/count;
        %Solve Average Frequency (1-sided)

```

```

A.avf(j)=sum(freq'.*A.avg(2:9))/sum(A.avg(2:9));
%Solve Average Period
A.avT(j)= 1./A.avf(j);

%Conduct South Beach Study
%Set dimensions of study area
dmn2=250;
dmx2=400;
rmn2=100;
rmx2=117;
B.avg=zeros(16,1);
count=0;
for d=dmn2:dmx2
    for r=rmn2:rmx2
        count=count+1;
        B.raw=double(squeeze(Cube.data(d,r,:)));
        %De-mean
        B.raw=B.raw-mean(B.raw);
        %Zero-pad
        B.raw(16)=0;
        %Sine Window
        B.sin=B.raw.*sin(pi*[0:15]'/15);
        %FFT
        B.fast=fft(B.sin)./N;
        %Spectral Energy
        B.energy=2*abs(B.fast).^2/df;
        %Sum Energy for Average Fr
        B.avg=B.avg+B.energy;
    end
end
%Solve Average Energy
B.avg=B.avg/count;
%Solve Average Frequency (1-sided)
B.avf(j)=sum(freq'.*B.avg(2:9))/sum(B.avg(2:9));
%Solve Average Period
B.avT(j)= 1./B.avf(j);

%Conduct Jetty Study
%Set dimensions of study area
dmn3=300;
dmx3=500;
rmn3=122;
rmx3=128;
C.tot=0;
C.st=0;
for r=rmn3:rmx3
    for d=dmn3:dmx3
        %Sum up total radar intensity

```

```

C.tot=C.tot+sum(double(squeeze(Cube.data(d,r,1:15))))/256;
    %Sum std dev for pixel

C.st=C.st+std(double(squeeze(Cube.data(d,r,1:15))),1);
    end
    end
    %Mean radar intensity (%) over study area x 15 time
steps
    C.int(j)=C.tot/((dmx3-dmn3)*(rmx3-rmn3)*15)*100;
    %Average std dev over study area
    C.dev(j)=C.st/((dmx3-dmn3)*(rmx3-rmn3));

    %Start next file
    tfile=tfile+100;
end
n=1;
for
j=length(Period.Nye.(Month))+1:length(Period.Nye.(Month))+24
    Period.Nye.(Month)(j)=A.avT(n);
    Period.South.(Month)(j)=B.avT(n);
    Intense.Jetty.(Month)(j)=C.int(n);
    Dev.Jetty.(Month)(j)=C.dev(n);
    n=n+1;
end
end

%Double running average
Period.Nye.(Month)(:,2)=filtfilt(ones(1,4),4,Period.Nye.(Month)(
:,1));
Period.South.(Month)(:,2)=filtfilt(ones(1,4),4,Period.South.(Mon
th)(:,1));
Intense.Jetty.(Month)(:,2)=filtfilt(ones(1,4),4,Intense.Jetty.(M
onth)(:,1));
Dev.Jetty.(Month)(:,2)=filtfilt(ones(1,4),4,Dev.Jetty.(Month)(:,
1));

save Period.mat Period
save Intense.mat Intense
save Dev.mat Dev
clear all

```

```

%Information for processing individual Months
% W=['152', '158', '167'];
% X=[771, 768, 772];
%
%
% file=0000
% addpath
(['Volumes/USB20FD/MissLinda/N04345040W12413416H120']);
% for i=1:771
%     I=imread([num2str(file,'%04.0f') '.jpg']);
%     Linda.H120(:,:,i)=I(:,:,1);
%     file=file+1;
% end
%
% file=0000
% addpath
(['Volumes/USB20FD/MissLinda/N04344743W12413215B158']);
% for i=1:768
%     I=imread(['N04344743W12413215B158' num2str(file,'%04.0f')
'.jpg']);
%     Linda.B158(:,:,i)=I(:,:,1);
%     file=file+1;
% end
%
% file=0000
% addpath
(['Volumes/USB20FD/MissLinda/N04345040W12413416H120']);
% for i=1:772
%     I=imread([num2str(file,'%04.0f') '.jpg']);
%     Linda.H120(:,:,i)=I(:,:,1);
%     file=file+1;
% end

%Set dimensions of study area, d=deg of theta, r=pixel radius
ymn=200;
ymx=225;
xmn=375;
xmx=400;
%Establish parameters for FFT
N=64;
dt=600/771;
df=1/(N*dt);
freq=[df:df:1/(dt*2)];
A1.avg=zeros(N,1);
count=0;
for y=ymn:ymx
    for x=xmn:xmx
        count=count+1;
    end
end

```

```

A1.raw=double(squeeze(Linda.B152(y,x,380:379+N)));
%De-mean
A1.mn=A1.raw-mean(A1.raw);
%Sine Window
A1.sin=A1.mn.*(sin(pi.*[0:(N-1)]./(N-1)))';
%FFT
A1.fast=fft(A1.sin)./N;
%Spectral Energy
A1.energy=2*abs(A1.fast).^2/df;
%Sum Energy for Average Fr
A1.avg=A1.avg+A1.energy;
end
end
%Solve Average Energy
A1.avg=A1.avg/count;
%Solve Average Frequency (1-sided)
A1.avf=sum(freq'.*A1.avg(2:N/2+1))/sum(A1.avg(2:N/2+1));
%Solve Average Period
A1.avT= 1./A1.avf;
semilogy(freq,A1.avg(2:N/2+1))

```